

Targeting the Water Network in Cyclin G-Associated Kinase (GAK) with 4-Anilino-quin(az)oline Inhibitors

Christopher R. M. Asquith,^{*[a, b]} Graham J. Tizzard,^[c] James M. Bennett,^[d] Carrow I. Wells,^[b] Jonathan M. Elkins,^[d, e] Timothy M. Willson,^[b] Antti Poso,^[f, g] and Tuomo Laitinen^[f]

Water networks within kinase inhibitor design and more widely within drug discovery are generally poorly understood. The successful targeting of these networks prospectively has great promise for all facets of inhibitor design, including potency and selectivity for the target. Herein, we describe the design and

testing of a targeted library of 4-anilinoquinolines for use as inhibitors of cyclin G-associated kinase (GAK). GAK cellular target engagement assays, ATP binding-site modelling and extensive water mapping provide a clear route to access potent inhibitors for GAK and beyond.

Inhibitor specificity and potency both present significant challenges in the development of kinase inhibitors and exploitation of kinase targets as potential therapies. The target profiles of commercial broad-spectrum kinase inhibitors are often challenging to rationalize in terms of direct molecular activity profiles. The large number of protein kinases present in the kinome (>500) makes this task even more difficult.^[1,2] Protein kinases that are functionally distinct yet retain key structural features can show overlapping ligand preferences, both with near and distant neighbours on the kinome tree.^[3]

A number of strategies have been explored to address the specificity problem in kinases.^[4] These approaches include exploitation of size of the kinase gatekeeper residue, the

disposition of the DFG-loop, chemotype selectivity, non-covalent interactions, salt-bridge, solvation, etc. Another method employed to obtain selective kinase inhibitors has been to target an allosteric site rather than the conserved ATP-binding site that is traditionally targeted and one that is unique to the kinase in question. Additionally, synthesizing inhibitors capable of covalent binding to a proximal cysteine has been successful to achieve selectivity over close family members. While each approach offers a possibility to achieve selectivity there is still a significant overall challenge to reach a successful endpoint. Identification and design of allosteric binders is challenging and most are found serendipitously.^[5] While inhibitors that modify the kinase covalently, first there has to be a residue capable of modification and then a way to assess the biological impact of that permanent modification.^[6]

There has been a growing appreciation that solvent specific effects can make significant contributions to ligand binding. The impact of these effects are however, usually retrospectively applied as a post-rationalization of the observed results.^[7-9] Development of software to model these effects has progressed with enveloping distribution sampling (EDS), free energy perturbation (FEP) theory and displaced-solvent functional (DSF) all recently being developed.^[10,11] However, the use of WaterMap by Schrödinger, Inc. has significantly advanced the ability to study direct solvation effects such as solvent replacement.^[12]

WaterMap couples molecular dynamics simulations with statistical thermodynamic analysis of water molecules within a protein structure. The method can provide insight not possible with traditional docking approaches. WaterMap was first used to rationalize the structure activity relationships of triazolylpurines binding to the A2A receptor.^[13] Specifically, *n*-butyl and *n*-pentyl substituents resulted in unanticipated potency gains, but these structure activity relationships could not be readily explained by ligand–receptor interactions, steric effects, or differences in ligand desolvation.

WaterMap has also been used in a number of kinase inhibitor programs including Src family kinases, Abl/c-Kit, Syk/ZAP-70, and CDK2/4 in order to rationalize kinase selectivity.^[13] Water modifications have also been shown to have a key effect

[a] Dr. C. R. M. Asquith
Department of Pharmacology, School of Medicine
University of North Carolina at Chapel Hill ■■■ Dear author, please add city ■■■ NC 27599 (USA)
E-mail: chris.asquith@unc.edu

[b] Dr. C. R. M. Asquith, C. I. Wells, Prof. T. M. Willson
Structural Genomics Consortium, UNC Eshelman School of Pharmacy
University of North Carolina at Chapel Hill
Chapel Hill, NC 27599 (USA)


[c] Dr. G. J. Tizzard
UK National Crystallography Service, School of Chemistry
University of Southampton
Southampton, SO17 1BJ (UK)

[d] J. M. Bennett, Dr. J. M. Elkins
Structural Genomics Consortium and Target Discovery Institute
Nuffield Department of Clinical Medicine, University of Oxford
Old Road Campus Research Building, Oxford, OX3 7DQ (UK).

[e] Dr. J. M. Elkins
Structural Genomics Consortium
Universidade Estadual de Campinas – UNICAMP
Campinas, São Paulo, 13083-886 (Brazil)

[f] Prof. A. Poso, Dr. T. Laitinen
School of Pharmacy, Faculty of Health Sciences
University of Eastern Finland
70211 Kuopio (Finland)

[g] Prof. A. Poso
University Hospital Tübingen
Department of Internal Medicine VIII, University of Tübingen
72076 Tübingen (Germany)

 Supporting information for this article is available on the WWW under <https://doi.org/10.1002/cmdc.202000150>

This article belongs to the Special Collection "Nordic Medicinal Chemistry 2019–2020"

in pivotal EGFR mutations showing resistance to afatinib and erlotinib.^[14] Molecular modelling studies on a PDGF-R β homology model using prediction of water thermodynamics suggested an optimization strategy for the 3,5-diaryl-pyrazin-2-ones as DFG-in binders by using a phenolic hydroxy group to replace a structural water molecule in the ATP binding site.^[15]

This water network principle has also been applied to bosutinib, as the 3-cyanoquinoline allows the compound to engage with a pair of conserved structured water molecules in the active site of Src.^[16] This post-rationalization approach hints at a more powerful use of this idea in the design of new inhibitors to exploit the water network hypothesis in its entirety to address both potency and selectivity.^[13]

In our work developing a selective chemical probe for cyclin G associated kinase (GAK), a member of the NAK subfamily.^[17-21] We observed two matched pairs of experimental results that did not fit with the expected structure activity relationship observed for GAK and the wider 4-anilinoquinoline scaffold (Figure 1).^[17]

GAK is involved in a plethora of biological processes including cell cycle progression,^[22] Parkinson's disease,^[23] osteosarcoma^[24] and prostate cancer.^[18,25] Although GAK is a historically under-studied kinase,^[26] recent probe development efforts identified potent and selective inhibitors of GAK from multiple chemotypes, including isothiazolo[5,4-*b*]pyridines,^[27-28] 4-anilinoquinolines and 4-anilinoquinazolines.^[17-20] These chem-

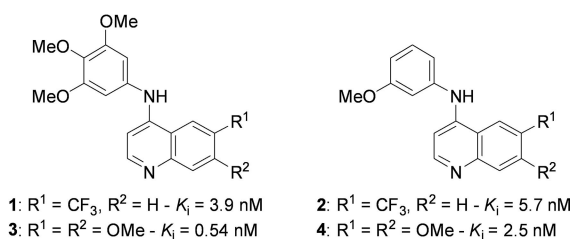


Figure 1. 4-Anilinoquinoline GAK inhibitor matched pairs with GAK activity shown.

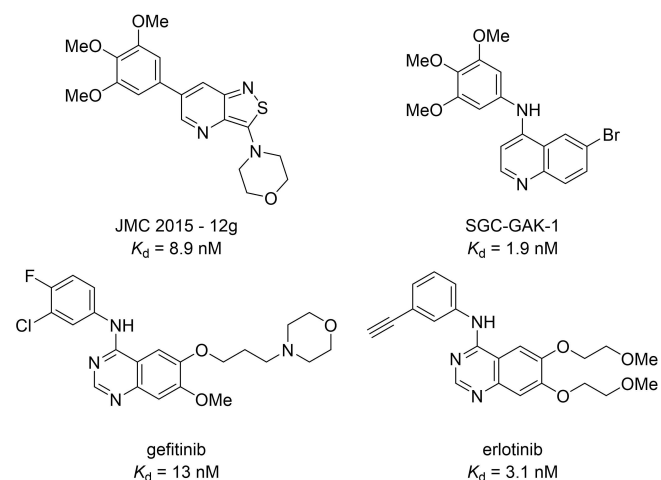


Figure 2. Previously reported GAK inhibitors.

ical probes may be used in the future to study of the biology of GAK.^[17,29] In contrast to probes, several FDA-approved drugs (Figure 2), including EGFR inhibitors gefitinib and erlotinib, have been reported to show off-target GAK activity in the low nanomolar range (Figure 2).^[30]

Results

The differently substituted matched pairs of trimethoxy- and *meta*-methoxy-substituted quinolines 1–4 showed potent binding to GAK with good NAK-family selectivity despite significant differences in both steric and electronic footprints.^[17] We looked for an alternative explanation for our observed equipotency and found through the application of WaterMap that there was a high-energy hydration site in the *p*-loop of the active site which is enabling both enhanced potency and NAK-family selectivity.

To further investigate this, we first looked at each NAK family member and observed that all have distinct water networks (Figure 3A–D). AAK1 and BIKE have a high degree of sequence identity in the kinase domain.^[21] There are some key residue differences located at the hinge region of each NAK family member: Leu125 (GAK)/Phe100 (STK16)/Tyr132 (BIKE)/Phe128 (AAK1), and Phe101 in STK16 in place of Cys126 (GAK)/Cys133 (BIKE)/Cys126 (AAK1). There are also alterations in the back pocket, where polar Thr123 and other bulkier residues like Leu98 (STK16) are located in case of GAK and Met130 and Met126 in case of BIKE and AAK1. Respectively, these alterations have significant impacts on the binding modes of inhibitors (Figure 3A, B).^[20] While the other three family members have lipophilic residues that have no ability to behave as a hydrogen bond donor/acceptors, GAK has Thr123 that can perform both functions. Moreover, the rotamer of Thr123 is likely fixed in place by an internal hydrogen bond to the backbone carbonyl group of Glu124 (Figure 3C, D).

This also gives rise to differences in the predicted water networks of the four NAK kinases (Figure 4A–D). However, only GAK has a high-energy hydration site likely due to small pit created by the interaction between Thr123 and Glu124 (Figure 4A). A hydration site is considered to be high in energy when the relative free energy value from WaterMap analysis has a high positive value, that is, 5.9 kcal/mol in case of GAK. There can be two cases when the hydration site has unfavourably high energy. First, water solvating hydrophobic enclosure such as in the case of GAK third strand of beta sheet (β 3) between Lys69 and Thr123. This type of cavity is energetically unfavourable (due to enthalpy) because water molecules cannot form a full complement of hydrogen bonds with surroundings. Second, is where the binding is entropically unfavourable, partly due to the closed nature of the hydration site. This is where water can form hydrogen bonds but suffers from reduced number of hydrogen bond configurations with protein groups and partner waters. Replacement of a water from such hydrations sites often may lead to improvement in affinity. Despite 17 sequence differences between GAK and AAK1/BIKE in the ATP binding domain,^[21] the only significant difference in

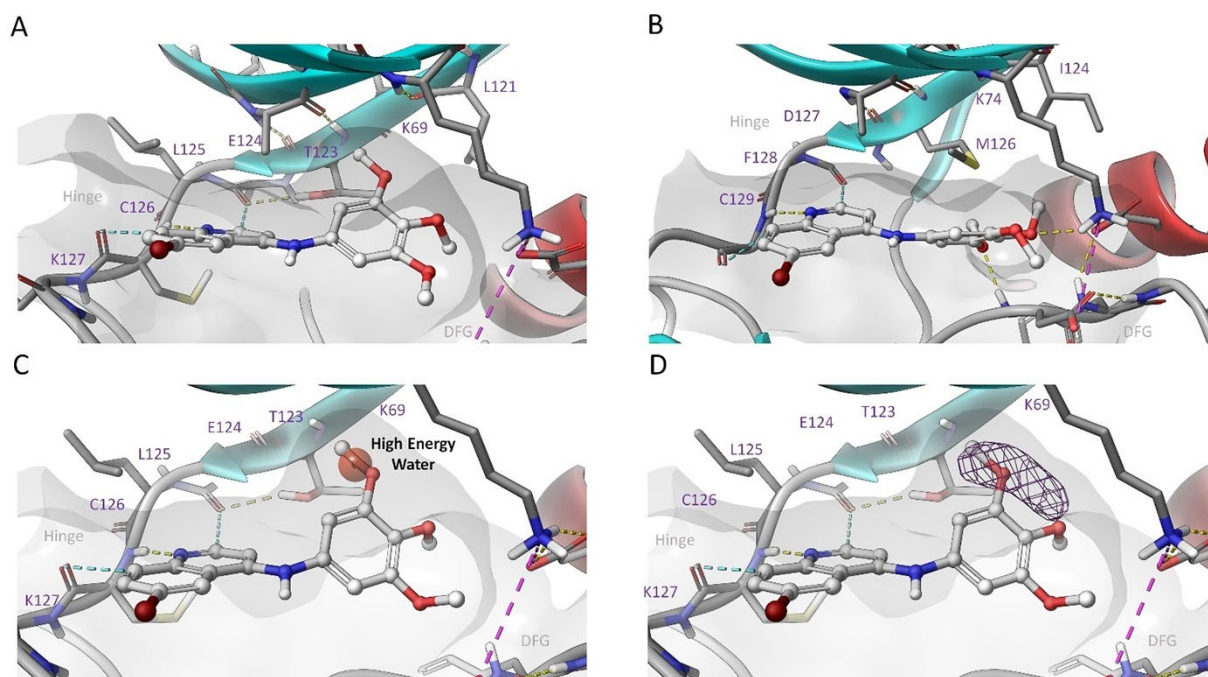


Figure 3. A) Additional space close to the β -sheet at the back pocket is occupied in the favourable docking pose of compound SGC-GAK-1. B) In comparison, in the case of AAK1, the corresponding back pocket area is filled by the methionine side chain (same location as Thr123 in GAK). C) An orange sphere shows the location of high-energy (5.9 kcal/mol) hydration site in GAK. D) The high-energy hydration site is actually dewetted (very low water occupancy) in WaterMap simulation.

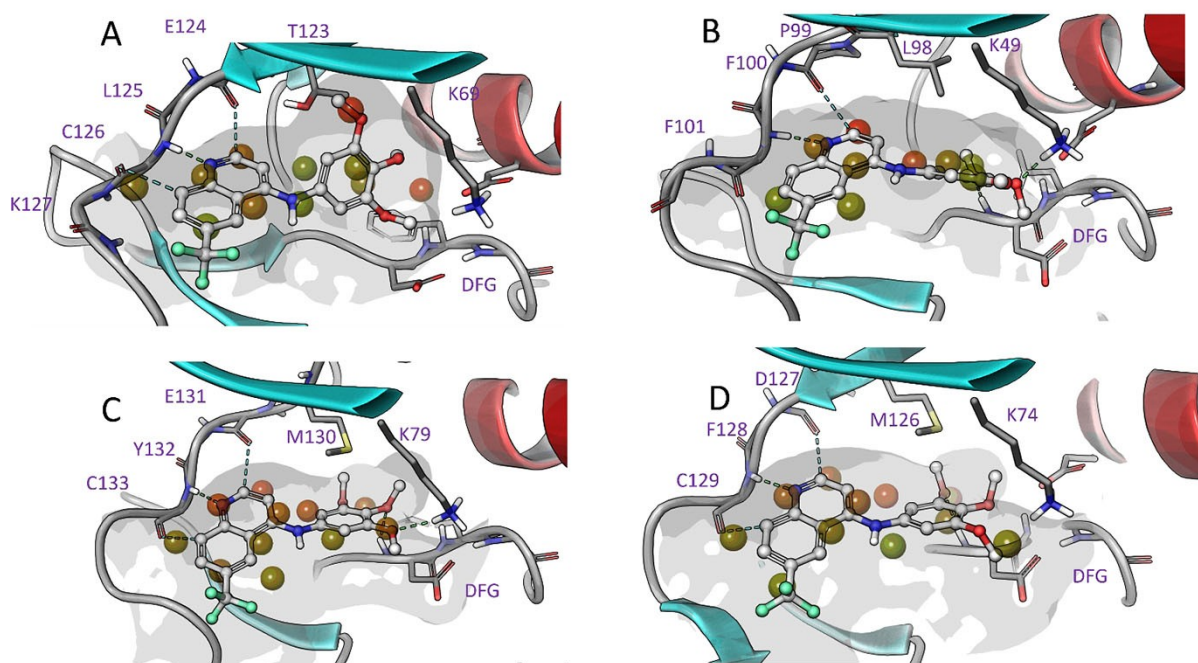


Figure 4. Molecular modelling of **1** in the water network of NAK family members by using WaterMap (high-energy waters are highlighted in red, lower-energy waters are in green): A) GAK (PDB ID: 5Y80); B) STK16 (PDB ID: 2BUJ); C) BIKE (PDB ID: 4W9X); D) AAK1 (PDB ID: 5TE0).

the water network is the presence of the high-energy water in the *p*-loop region (Figure 3A–D). The most structurally diverse NAK family member STK16 has 64 differences in the kinase

sequence compared to the other NAK kinases in the ATP binding domain. STK16 has a significantly different water network compared to the other NAK family members but does

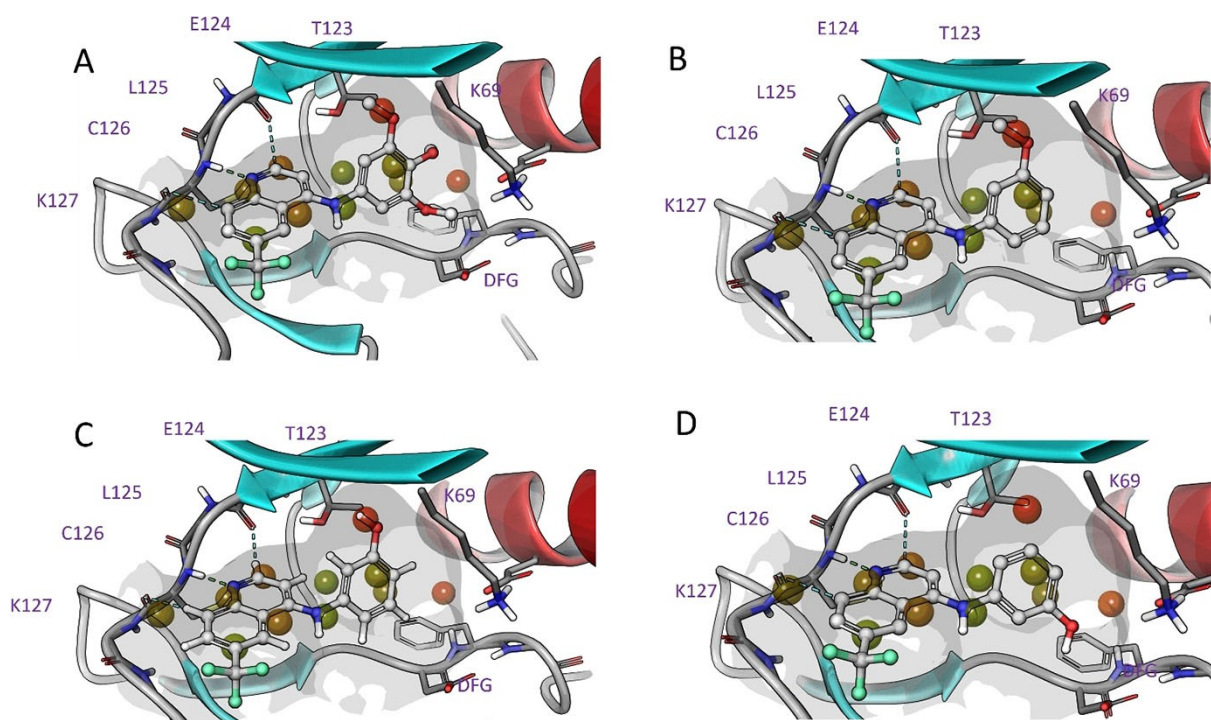


Figure 5. WaterMap modelling of GAK where high-energy waters are highlighted in red, lower energy waters are in green (PDB ID: 5Y80), with A) 1; B) 4; C) 5 and D) 5.

possess a high-energy water that is in a 7 Å out of plane orientation related to the GAK protein structure (Figure 4A, D).

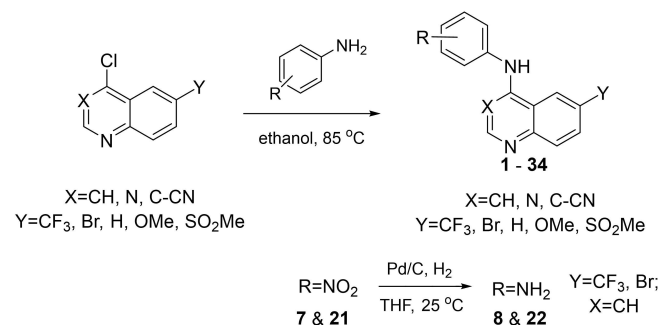
Through a series of prospective simulations using WaterMap we identified that this additional high-energy hydration site next to the spine of the ATP binding pocket makes the shape of the GAK binding back pocket rather different to other NAK kinases studied (Figure 4).^[31] A hydrophobic furrow is formed next to Thr123, where the side chain is hydrogen bonded to the backbone carbonyl group of Glu124, and is rather small in size overall. While in case of other NAK kinases there is either a bulky methionine (AAK1 and BIKE) or Ile110 in the case of STK16 (Figure 3A, B). As a consequence, in the case of GAK, this hydrophobic site can be readily occupied by a ligand substituent without side chain rearrangements.

The water network simulation of the 6-(trifluoromethyl)-*N*-(3,4,5-trimethoxyphenyl)quinolin-4-amine (1) versus *meta*-methoxy derivative 2 demonstrated plausibility of the high-energy water displacement to explain the almost equipotent high GAK activity (Figure 5A, B). The slight increase in potency could be attributed to the rearrangement of the catalytic lysine to sit between the two additional methoxy groups in 1. Reforming of the water contacts by removal of the methyl group from the methoxy group (5) showed an encouraging ability to lock the phenolic –OH in place in the preferred docking pose (Figure 5C). Compound 5 could also be forced to adopt a higher energy conformation where the –OH interacts with the catalytic lysine (Figure 5D). The new H-bond lysine interaction is not compensating the two H-bonds replacing the high-energy

water. Although metabolic liability of a phenolic –OH is well known, it is a strong proof of concept substitution.^[32]

To further probe the structural requirements for GAK activity and the water network, we synthesized a series of analogues (Scheme 1). 4-Anilinoquinolines were prepared by heating the corresponding 4-chloroquinoline derivative and substituted aniline in ethanol with Hünigs base and refluxed overnight.^[17–20,33–34] The synthesis afforded products 1–34 in good yield (58–86%). Interestingly, the more activated reaction to 6-bromo-4-chloroquinoline-3-carbonitrile was completed in two hours to afford 31 in good yield (69%). The hydrogenations of the nitro derivatives 7 and 21 to form 8 and 22 were routine with good to excellent yields (69 and 94% respectively).

The compounds were initially screened for activity on the kinase domains of all four members of the NAK family members



Scheme 1. General synthetic route to analogues 1–34.

(GAK, AAK1, BMP2 K, and STK16) using a time-resolved fluorescence energy transfer (TR-FRET) binding displacement assay in a 16-point dose response format to determine the inhibition constant (K_i). The compounds were then screened in a cellular target engagement assay nanoluciferase (nanoLuc) bioluminescence resonance energy transfer (BRET; NanoBRET) assay for GAK.^[17–18,35–36] The sensitive nature of the assay allows a complimentary comparison to the TR-FRET to observe subtle trends in the GAK inhibition profile.

The background provided by 1–4 and Figure 3A–D led us to probe around the 6-trifluoromethyl substituted quinolines with some small modifications looking for potential hydrogen bond interactions to further boost the initial potency in the structure activity relationships observed (Figure 1).^[17] The trimethoxy compound 1 demonstrated high affinity for GAK and good selectivity against the rest of the NAK family members. A switch from the trimethoxy- (1) to the *meta*-methoxy-substitution (2) showed almost equipotency consistent with previous reports.^[17]

The GAK NanoBRET showed an almost 3-fold drop in cellular target engagement from 1 to 2. This effect is still impressive as the *meta*-methoxy derivative 2 is able to substitute the trimethoxy functionality despite not occupying the same space orientation.^[16] A switch from *meta*-methoxy (2) to *meta*-hydroxy (5) showed a slight increase in GAK binding but not as significantly as the modelling predicted (Table 1).

We then switched to a *meta*-nitro group (6) or *meta*-amino group (7) to investigate the possibility of forming multiple hydrogen bonds.^[37] However, both 6 and 7 proved to be relatively ineffective with a 45- and 25-fold decrease in GAK binding respectively and a low micromolar cellular target engagement. The addition of two methyl groups to the amine (8) demonstrated a 5-fold decrease in GAK potency (K_i = 650 nM). The removal of the trifluoromethyl group of 7 and 8 to

form 9 and 10 respectively showed the same trend in GAK potency but a 4-fold increase in selectivity (8 vs. 10). We returned to the hydroxy moiety and inserted a methyl linker between the aniline with the aim to effectively generate a hydrogen bond interaction with Thr123. The methanol analogues 11 and 12 proved to be 10-fold weaker on GAK, likely due to spatial constraints in the top pocket of the ATP binding site.

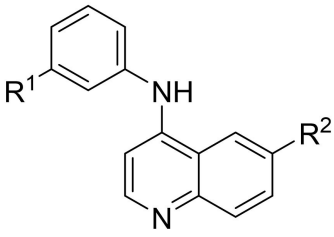
The NAK family selectivity pattern observed with 1–5 hinted at a potential water displacement. With this in mind we explored a series of *meta*-methoxy and *meta*-hydroxy matched pairs (Table 1). Compound 2 has a favourable NAK family profile towards GAK and has previously been shown to have a narrow spectrum profile across the kinome.^[19] The 6-bromoquinoline (13–14) is the optimal substituent for GAK inhibition on this scaffold (Table 2).^[17–19,34] This substitution offers optimal GAK binding in the solvent exposed mouth of the ATP binding site and potent GAK inhibition at lower concentrations. The switch from the trimethoxy to the *meta*-methoxy substitution (13) was equipotent to the binding of 2 on GAK; but with a corresponding drop off in NAK selectivity and NanoBRET activity. The switch from 13 to the hydroxy substituted compound 14 shows an almost threefold increase in K_i which was more pronounced in the cellular assay with an almost tenfold increase from an IC_{50} of 218 to 26 nM.

The removal of the 6-bromo to the unsubstituted quinoline analogue 15 resulted in a tenfold drop in potency of *meta*-methoxy (15); with the hydroxy (16) only giving a limited increase in GAK affinity. The NanoBRET results for 15 and 16 were weaker but consistent with the trend observed. The 6-methoxy-*N*-(3-methoxyphenyl)quinolin-4-amine (17) showed good activity that tracked with the previously reported trimethoxy derivative.^[17] However, the switch from trimethoxy to *meta*-

Table 1. Investigation of matched pairs of *meta*-substituted quinolines.

Cmpd	R ¹	R ²	R ³	R ⁴	R ⁵	Binding displacement assay K_i [μ M] ^[b]				NAK selectivity ^[c]	GAK NanoBRET IC_{50} [μ M] ^[d]
						GAK	AAK1	BMP2 K	STK16		
1 ^[a]	OMe	OMe	OMe	H	CF ₃	0.0039	54	> 100	17	4300	0.17
2 ^[a]	OMe	H	H	H	CF ₃	0.0057	14	23	18	2500	0.48
5	OH	H	H	H	CF ₃	0.0047	2.6	5.8	3	550	0.23
6	NO ₂	H	H	H	CF ₃	0.21	> 100	> 100	> 100	480	> 5
7	NH ₂	H	H	H	CF ₃	0.12	6.8	17	45	57	2.7
8	NMe ₂	H	H	H	CF ₃	0.65	> 100	> 100	13	20	> 5
9	NO ₂	H	H	H	H	0.17	38	> 100	> 100	220	> 5
10	NMe ₂	H	H	H	H	0.97	29	> 100	> 100	30	> 5
11	CH ₂ OH	H	H	H	CF ₃	0.06	10	15	20	170	1.7
12	H	H	H	CH ₂ OH	CF ₃	0.041	8.5	16	5	120	2.3

[a] Consistent with previous report[17]; [b] TR-FRET-based ligand binding displacement assay; [c] (NAK/GAK); [d] IC_{50} [μ M] ($n=2$, mean).

Table 2. Comparative results based on compound 1 and 2.


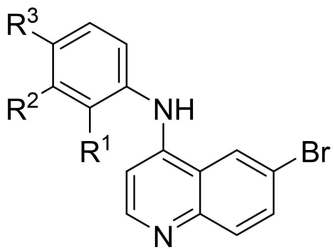
Cmpd	R ¹	R ²	Binding displacement assay Ki [μM] ^[b]				NAK selectivity ^[c]	GAK NanoBRET IC ₅₀ [μM] ^[d]
			GAK	AAK1	BMP2 K	STK16		
2 ^[a]	OMe	CF ₃	0.0057	14	23	18	2500	0.17
5	OH	CF ₃	0.0047	2.6	5.8	3.0	550	0.48
13	OMe	Br	0.0029	3.0	7.0	32	1000	0.22
14	OH	Br	0.0012	0.50	2.0	5.7	420	0.026
15	OMe	H	0.027	25	> 100	> 100	930	0.60
16	OH	H	0.012	6.6	30	> 100	550	0.44
17	OMe	OMe	0.0079	9.1	26	> 100	1300	0.17
18	OH	OMe	0.0057	1.6	7.3	27	280	0.11
19	OMe	SO ₂ Me	0.030	23	19	> 100	630	1.0
20	OH	SO ₂ Me	0.023	5.1	3.5	1.2	520	1.0

[a] Consistent with previous report;^[17] [b] TR-FRET-based ligand binding displacement assay; [c] (NAK/GAK); [d] IC₅₀ [μM] (n = 2, mean).

methoxy substitution resulted in a NAK selectivity drop of sixfold.^[16] The switch to the hydroxy moiety (18) gave only a slight increase in GAK activity and the same NAK selectivity as the previously reported trimethoxy compound 3. This trend was repeated in the GAK NanoBRET. The 6-methyl sulfone *meta*-methoxy (19) was a weaker GAK binder consistent with previous structure activity relationships observed on this scaffold.^[17] The trend observed between 13 and 14 provided the strongest evidence yet that the potential water was being displaced (Table 2). A further switch to the nitro substitution with the 6-bromoquinoline 21, was ten times more active than

the corresponding 6-trifluoromethyl compound 6 (Table 3). This further supports the rationale that the 6-trifluoroquinoline does not allow the optimal orientation when compared to the 6-bromoquinoline.

However, surprisingly the *meta*-amino group of the 6-bromo compound 22 was three times less potent on GAK than 7. The dimethyl amino aniline derivative 22 was broadly in line with expectations with similar potency to the 6-trifluoromethylquinolines 7 and 8. The switch from an oxygen atom to a nitrogen atom reduces GAK potency which would suggest that the electronegativity of the oxygen atom is required for the

Table 3. Investigation of water pocket with isosteric replacement of *meta*-methoxy on the 6-bromoquinoline.


Cmpd	R ¹	R ²	R ³	Binding displacement assay Ki [μM] ^[a]				NAK selectivity ^[b]	GAK NanoBRET IC ₅₀ [μM] ^[c]
				GAK	AAK1	BMP2 K	STK16		
13	H	OMe	H	0.0029	3.0	7.0	32	1000	0.22
14	H	OH	H	0.0012	0.50	2.0	5.7	420	0.026
21	H	NO ₂	H	0.056	40	> 100	> 100	710	> 5
22	H	NH ₂	H	0.67	8.9	23	17	13	1.9
23	H	NMe ₂	H	0.37	7.5	> 100	28	20	2.3
24	H	CH ₂ OH	H	0.017	4.6	10	11	270	1.3
25	H	OCH ₂ O		0.035	5.2	12	10	150	> 5
26	H	CH ₂ OCH ₂		0.12	4.3	9.4	24	36	> 5
27	OCH ₂ O		H	0.0019	> 100	> 100	> 100	53000	0.022
28	CH ₂ OCH ₂		H	0.13	11	25	15	82	> 5

[a] TR-FRET-based ligand binding displacement assay; [b] (NAK/GAK); [c] IC₅₀ [μM] (n = 2, mean).

optimal replacement of the water.^[38] The *meta*-methanol derivative **24** showed only a limited improvement towards GAK binding compared to the 6-trifluoromethyl (**11**).

We then explored how torsional strain on the methoxy orientation and constrained ring systems would affect the GAK activity profile. The fused ring systems (**25–28**) demonstrate how sensitive the water network is and how an island of activity can be achieved. Compounds **25** and **27** demonstrate the same effect as **1** and **2**. The 3,4 connectivity (**25**) vs 2,3 connectivity (**27**) showed a preference for the orthogonal plane angle and an ability to accommodate this in the ATP pocket. However, with **25**, the rotational energy penalty combined with constraints at the 4-position accounts for a 14-fold drop in potency on GAK (**25** vs. **27**).

The drop is more severe with the mono-substituted central oxygen which produces two equipotent compounds (**26** and **28**) regardless of positioning (Figure S1). The result was the identification of a potent cell active GAK inhibitor (**27**).

We then looked at the conformation of the compounds and the influence this has on the potential water displacement (Table 4). Switching from the quinoline *meta*-methoxy aniline (**13**) to quinazoline (**29**) results in a 4-fold penalty, likely related to the flattening of the molecules conformation. The corresponding *meta*-hydroxy analogue **30** was equipotent with **29** in GAK binding, likely due to the inability to effectively form the hydrogen bond to replace the water molecule due to the planer character of the compound. Switching back to the 6-bromoquinoline, *meta*-tetrazole **31** with the potential to form multiple hydrogen bonds, mimicked the nitro substitution (**21**) in potency and selectivity despite occupying a large space. The three compounds pentafluorosulfanyl (**32**),^[39] *tert*-butoxy (**33**) and the *tert*-butyl (**34**) were likely too large and lipophilic with each demonstrating GAK binding (K_i) between 2 and 3 micromolar. This highlights the requirement for small, precisely

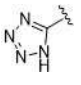
oriented hydrogen bond donors with correct torsional strain to effectively displace the water and form a strong interaction.

In order to rationalize the results observed (Table 1–4) we modelled key compounds SGC-GAK-1, **13**, **14**, and **25–28** in the GAK ATP competitive active site with Glide module of Schrödinger Maestro suite (Figure S1).^[40] We observed through docking that unlike SGC-GAK-1, the *meta*-methoxy derivative (**13**) was not able to form an interaction with the catalytic lysine (Lys69). This runs counter to the observed GAK binding where SGC-GAK-1 and **13** have near equipotency despite this interaction deficit, suggesting other factors including the water network.

The docking of quinazoline **29** demonstrated a lack of the correct orientation to form optimal binding to GAK (Figure S1). The docked *meta*-hydroxy (**14**) proposed direct interaction with the alcohol altering the through molecule orientation to form a rarely reported sigma hole interaction (halogen bond) directly with the 6-position bromine mediated through a water molecule bound next to the carbonyl from Leu46 (Figure S2).^[41] During our investigations this result was not observed with any other analogue. The 5-membered dioxane derivative **27** demonstrated the ability to form an optimal fit while still displacing the water (Figure S1). Surprisingly none of the other closely related derivatives **25**, **26** and **28** were able to achieve this (Table 3).

The WaterMap simulations demonstrate the ability of the most potent GAK inhibitors in the NanoBRET SGC-GAK-1, **13**, **30** and **27** to displace the high-energy water present in the hydrophobic pocket. The displacement of this high-energy water provides a significant boost of binding affinity. SGC-GAK-1 was able to displace the water and interact with the catalytic lysine (Figure 6A). The *meta*-methoxy derivative **13** was able to interact with the catalytic lysine but preferentially chose to displace the water (15/15 simulations; Figure 6B). The WaterMap simulation also demonstrated that the quinazoline **30** had a

Table 4. Investigation of water pocket with isoteric replacement of *meta*-methoxy group and different hinge binders.

Cmpd	R ¹	X ¹	Binding displacement assay Ki [μM][a]				NAK selectivity ^[b]	GAK NanoBRET IC ₅₀ [μM] ^[c]
			GAK	AAK1	BMP2 K	STK16		
12	OMe	CH	0.0029	3.0	7.0	32	1000	0.22
29	OMe	N	0.011	0.39	1.3	5.5	35	0.76
30	OH	N	0.012	0.16	0.75	3.6	13	1.0
31		CH	0.24	5.7	41	6.0	24	> 5
32	SF ₅	CH	4.9	> 100	> 100	> 100	> 20	> 5
33	O ^t Bu	CH	2.2	15	> 100	12	5	> 5
34	^t Bu	CH	2.6	> 100	> 100	> 100	> 38	> 5

[a] TR-FRET-based ligand binding displacement assay; [b] (NAK/GAK); [c] IC₅₀ [μM] (n = 2, mean).

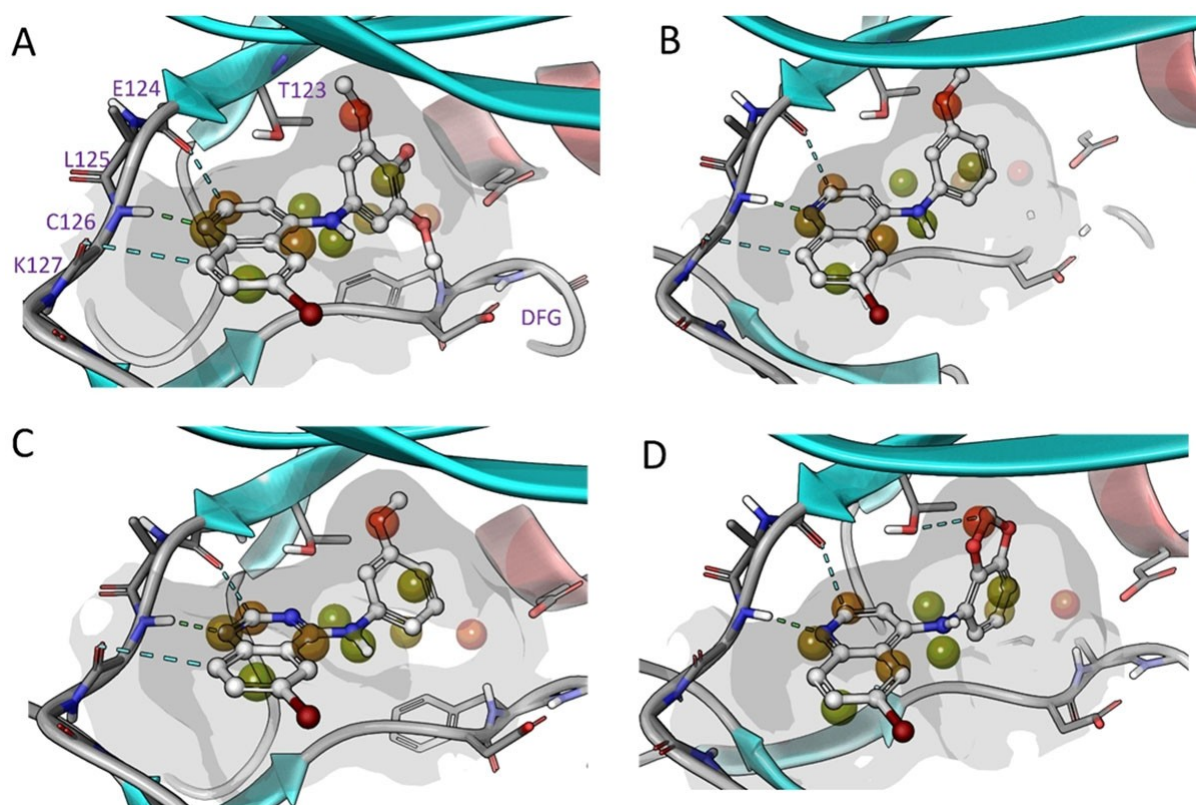


Figure 6. Main WaterMap hydration sites overlaid with selected ligands A) SGC-GAK-1, B) **13**, C) **30** and D) **27** in the GAK ATP binding domain.

more flexible conformation and hence was able to only partially displace the water molecule (Figure 6C). The 5-member dioxane number was set up in the correct orientation to displace the water molecule (Figure 6D). Interestingly, while **25**, **26** and **28** were good binders they were not well set up to displace the high-energy water or form key interactions in the ATP binding site of GAK (Figure S1).

In order to investigate the bound water hypothesis further and to further elucidate what constitutes a high and low energy water within the GAK kinase domain we searched for 'dry areas' within the ATP binding pocket. These are portions of the receptor active site that are so unfavourable for water molecules that a void is formed there. These are uncommon but have been theoretically and experimentally been observed.^[42]

The WaterMap analysis of APO structure of GAK (Figure 7A) and ligand binding form (Figure 7B) of GAK demonstrated that water bound to the high-energy pocket had a low relative occupancy of 0.42 in case of APO and 0.53 in case of gefitinib bound, respectively. These low occupancies highlight that there is space, but the positioning of the water is sub-optimal even though a pocket of space available.

Hydration site analysis with bound gefitinib (Figure 7C) showed the pocket present but is only partly occupied by the aniline portion of gefitinib. When gefitinib is switched for SGC-GAK-1 (Figure 7D) the hydration site analysis indicates that all the sites are occupied with ligand substituent arms on the

trimethoxyaniline portion of the molecule. This provides further explanation for high affinity and enhanced specificity of SGC-GAK-1 and the current series of ligands. An interesting feature of the GAK ATP binding site is that Thr123 is not able to occupy that space at roof of the back pocket which is the origin of this 'dry' area.

The observed torsional effects of the aniline to quin(az)oline ring system observed with **13** vs **29** were further explored by solving a series of small molecule crystal structures of **13**, **14**, **25**, **27** and **29** (Figure 8). The chloride salts of **13**, **14**, **25** and **27** crystallized and as expected, hydrogen bonding between the amine (and alcohol; **13**), amine donors and chloride counter-ion are the dominant intermolecular interactions within these structures, leading to simple hydrogen bonded 1D chains in each case. Additionally, **13** and **25** crystallize as hydrates with disordered water molecules in channels parallel to the *a*- and *c*-axes respectively resulting in more complex 3D hydrogen bonded networks. Only **29** crystallizes as a pure substance and also forms 1D hydrogen bonded chains *via* the aniline and quinazoline 1-position nitrogen. Structures **13** and **29** crystallize with two independent molecules in the asymmetric unit related by approximate inversion in both cases. The C–N–C–C torsion angles of **12**, **13**, **25**, **27** and **29** occur in narrow range between $\pm 32.4(8)^\circ$ – $\pm 61.62(18)^\circ$ with **12** and **27** displaying torsion angles $> \pm 50^\circ$. The functional groups of the aniline moiety are positioned above the rotation axis of the aniline ring

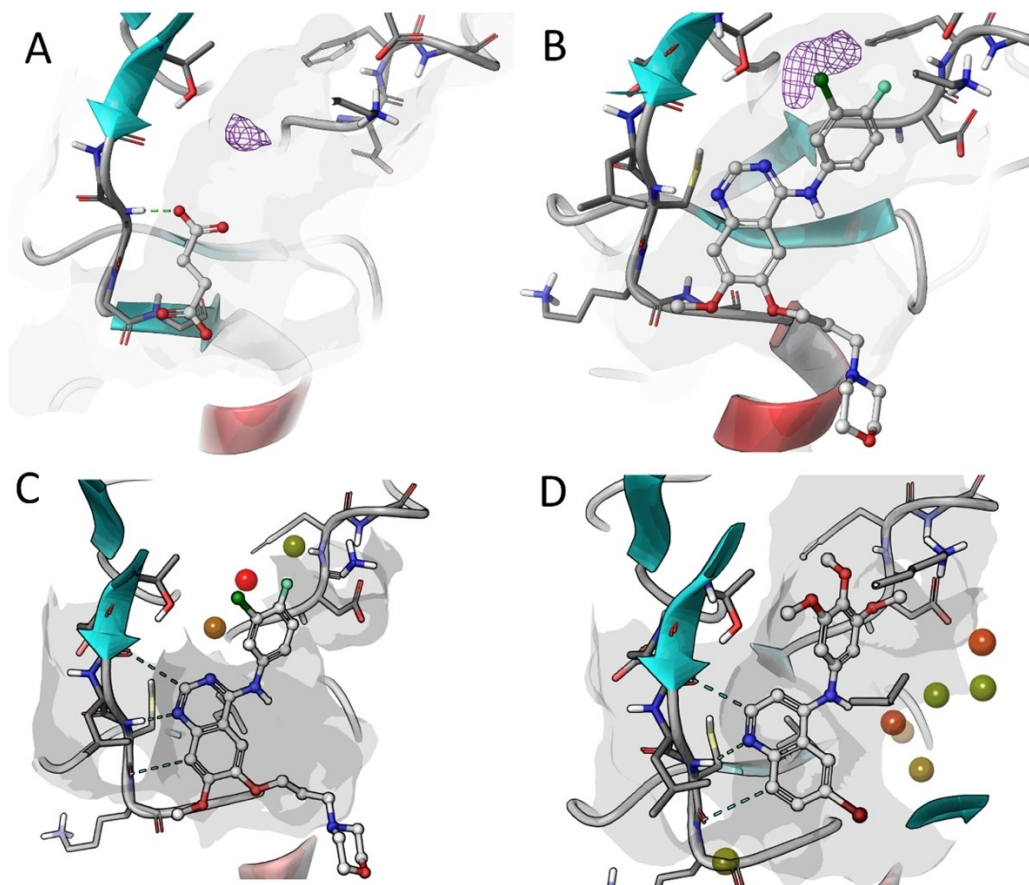


Figure 7. A) GAK APO structure WaterMap (PDB ID: 4C38); B) showing dewetted area extracted from WaterMap simulation overlaid with gefitinib (PDB ID: 5Y80); C) WaterMap simulation with gefitinib bound to GAK (PDB ID: 5Y80); D) WaterMap simulation with SGC-GAK-1 bound to GAK (PDB ID: 5Y80).

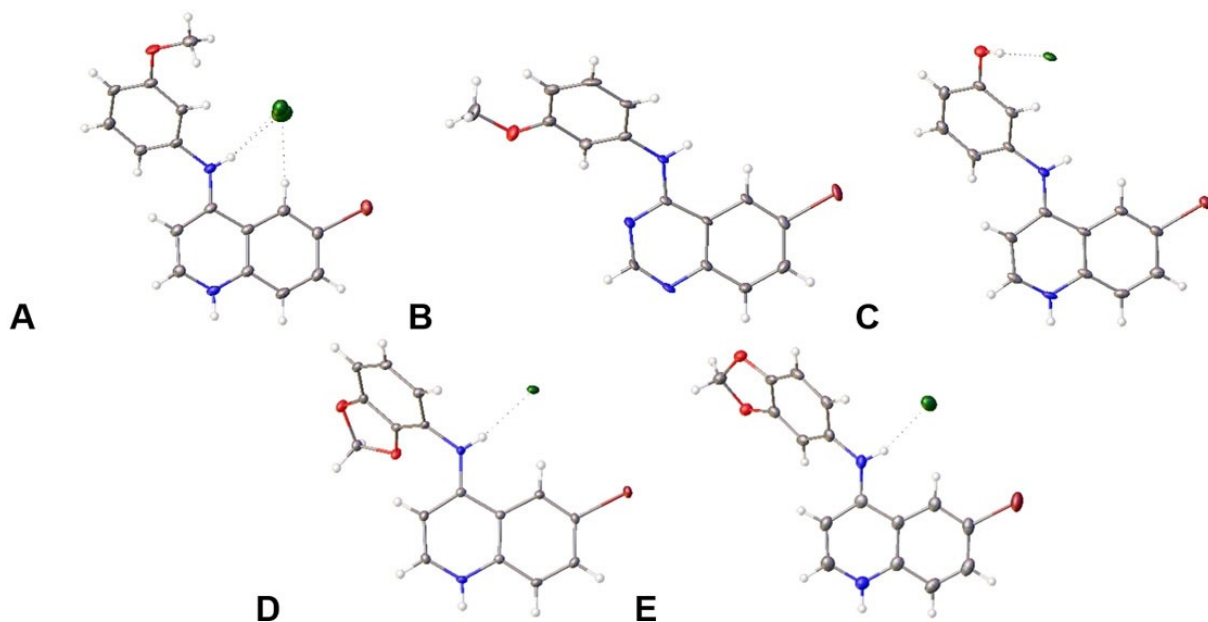


Figure 8. Crystal structures of A) 13, B) 29, C) 14, D) 27 and E) 25. ADP ellipsoids are displayed at 50% probability. Counter ions are shown but solvent molecules are not shown for clarity.

of 12 and 13 whereas they are below the axis of rotation in 25, 27 and 29.

Discussion

The tractability of protein kinases is well known, with more than 50 inhibitors targeting the ATP binding site of kinases approved for use in the clinic.^[43] However, most of these drugs leverage the conservation of the ATP binding pocket across kinases to increase their clinical efficacy.^[31] These multikinase inhibitors, although effective, would not be well suited outside oncology indications. Development of kinase inhibitors for new treatments outside of oncology will require inhibitors with significantly improved potency and selectivity profiles.^[44] Novel approaches to tackle this issue are urgently required in order to effectively develop highly selective and potent kinase inhibitors to target the conserved ATP binding site outside oncology indications.

Several tools to achieve this aim are available with binding assays enabling rapid, accurate and robust method to assess potency and potentially wider selectivity of ATP-competitive kinase inhibitors.^[45–46] These ligand binding displacement assays also provide an accepted direct measurement of kinase inhibition in drug optimization of ATP binding site inhibitors.^[45] This is a particularly acute point in the case of more neglected kinases such as GAK where there are currently no robust and validated enzyme activity assays.^[47]

The water network is not a novel concept but has so far attracted limited attention. This is partially due to the fact that targeting and predicting the water network is difficult and, in some cases, not precise enough. WaterMap and other solvent prediction systems have attempted to bridge this gap while other efforts including the *KILFS* database have attempted to map the ATP binding sites across the kinome.^[48] Direct use of WaterMap has been demonstrated to enable, assess and design selectivity within PI3 K subtypes (α , β , γ , and δ) which have highly similar ATP binding sites. The critical role of water molecules in molecular recognition is under recognized and could provide a useful rationalization to drive down potency and improve selectivity.^[49]

WaterMap analysis of the GAK ATP binding site suggested that a coordinated water network in the protein pocket spans the region proximal the aniline and the 6-position of the ring

system. However, one poorly coordinated higher energy water molecule within this network is able to be targeted and displaced. The effect of this displacement leads up to a tenfold boost due to entropic and enthalpic contributions to the free energy of binding (Figures 4,–6). These models suggest that a water network within the GAK active site plays a critical role in defining the relative affinity of quinoline ligands. Extension of this model to other NAK family members demonstrates why the 4-anilinoquinoline is significantly more potent on GAK compared to the other NAK family members that lack that higher energy water molecule in the lipophilic pocket of the ATP binding site within GAK (Figures 3 and 4). The influence of different substituents on the preferred fragment pose was analysed by various computational approaches. The orthogonal off-targets between 1 and JMC 2015-12 g led us to postulate that the replacement of water molecules results in different flipped binding modes between the two scaffolds (Figure 9A, B). This was supported by several computational studies in the literature,^[49–50] in addition to a series of oxindole derivatives demonstrating selective DYRK inhibition by a water induced flipped binding mode.^[51] Our observations were further bolstered by a recently solved co-crystal structure of gefitinib in GAK showing the same high-energy water being displaced (Figure 9C).^[52]

In summary, we have identified and optimized an island of activity within the ATP binding pocket of GAK by displacement of a high-energy water within the lipophilic pocket. The water molecules that occupy the ligand binding pocket prior to small-molecule binding to a protein pocket play a significant role and can be considered as principal source of binding energy. These water molecules occupy certain hydration sites inside the pocket and are either energetically favourable or unfavourable in comparison to the bulk water. If the total energy of a hydration site is positive e.g. it is unfavourable, the replacement of this water will result in a binding affinity boost. A hydration site may be high in energy for multiple reasons, for example if a water is not able to form hydrogen bonds within the site enthalpic penalty results. Entropic penalty can exist when degrees of freedom are unfavourable for water compared to bulk waters. It is also common that a pocket water is transformed to be unfavourable if it is trapped or the degrees of freedom are limited when a small molecule is introduced to the binding site.

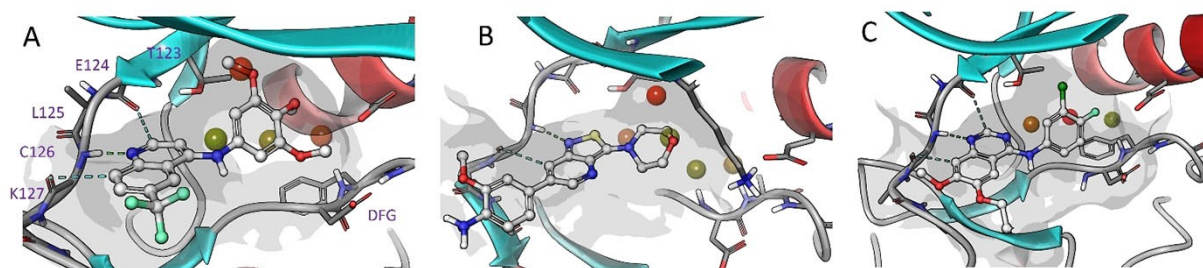


Figure 9. Selected WaterMap hydration sites overlaid with of A) 1 docked (PDB ID: 5Y80), B) JMC 2015-12 g retained at adenosine binding site of GAK (PDB ID: 4Y8D) and C) Gefitinib retained at adenosine binding site (PDB ID: 5Y80).

In this study we have used WaterMap from Schrödinger to conduct hydration site analysis for family NAK kinases in order to explain ligand affinity further than simple crude scoring functions used in straightforward docking can achieve.^[42,53–56] The WaterMap software conducts statistical mechanics based on short molecular dynamics. This simulation describes the thermodynamic properties to estimate the energies of the hydration sites. This estimation is usually computed for the pocket without ligand to evaluate possible hydration sites but can be also calculated with ligand. However, such short simulations keeping the protein rigid is highly dependent on the conformation of the protein and results are less valid in the case of arbitrary changes in protein conformations. Fortunately, the case of the NAK family kinases is well suited for hydration site analysis thus binding conformations are mapped by several high-resolution x-ray structures resulting in good overall convergence of the ligand dockings.

This method can be used to further optimize GAK inhibitors for potential *in vitro* and *in vivo* usage.^[20,57] Extension of this model to other NAK family members or more distantly related kinases could lead to computational models that predict wider kinome selectivity.

Experimental Section

Modelling

Molecular modelling: Molecular modelling was performed using Schrödinger Maestro software package (Small-Molecule Drug Discovery Suite 2018-4, Schrödinger, LLC, New York, NY, 2018) Prior to docking simulations structures of small molecules were prepared using and the LigPrep module of Schrödinger suite employing OPLS3e force field.^[55] In the case of GAK and other NAK family kinases there are a number of co-crystal structures available representing various ligand binding conformations, showing flexibility in the position of so-called the p-loop and C-helix region. Suitable docking templates were searched using LPDB module of Schrödinger package and carrying out visual inspection of available experimental structures with assistance of LiteMol plug-in available at website of UniProt database. Selected coordinates (PDB IDs: 4Y8D and 5Y7Z) have been co-crystallized with at resolution of 2.1 Å and 2.5 Å respectively with a small molecule inhibitors.^[26,52] The PDB structure of GAK was H-bond optimized and minimized using standard protein preparation procedure of Schrödinger suite. The ligand docking was performed using SP settings of Schrödinger docking protocol with softened vdw potential (scaling 0.6). In order to improve convergence of docking poses a hydrogen bond constraint to mainchain NH of hinge residue was required, as experimentally observed in the case of quinoline/quinolizine scaffolds (for example NH of C126 in the case of GAK). The grid box was centered using coordinate center of the core structure of corresponding x-ray ligand as template. Graphical illustrations were generated using, Maestro, and PyMOL software of Schrödinger.

Hydration site analysis: Hydration site analysis calculated with WaterMap (Schrödinger Release 2018-4: WaterMap, Schrödinger, LLC, New York, NY, 2018.). The structure of GAK (PDB ID: 4Y8D and 5Y7Z) was prepared with Protein Preparation Wizard (as above).^[27,52] Water molecules were analysed within 6 Å from the docked ligand, and the 2 ns simulation was conducted with OPLS3e force field.^[55]

Biology

Cellular NanoBRET target engagement assay: Screening was performed as previously described.^[17] Briefly, the N-terminal Nano Luciferase/GAK fusion (NL-GAK) was encoded in pFN31K expression vector, including flexible Gly-Ser-Ser-Gly linkers between NL and GAK (Promega Madison, WI, USA).¹ For cellular NanoBRET target engagement experiments, the NL-GAK fusion construct was diluted with carrier DNA-pGEM-3Zf(–) (Promega, Madison, WI, USA) at a mass ratio of 1:10 (mass/mass), prior to adding FuGENE HD (Promega). DNA:FuGENE complexes were formed at a ratio of 1:3 (µg DNA/µL FuGENE HD) according to the manufacturer's protocol (Promega). The resulting transfection complex (1 part, volume) was then gently mixed with 20 parts (v/v) of HEK-293 cells (ATCC) suspended at a density of 2×10^5 cells/mL in DMEM (Gibco) + 10% FBS (Seradigm/VWR) followed by incubation (37 °C/5% CO₂) for 24 hours. After 24 hours HEK293 NL-GAK transfected cells were detached from flasks (0.05% Trypsin-EDTA or TrypLE) (Gibco) and re-suspended at a concentration of 2×10^5 cells/mL in Opti-MEM media (Gibco).

Cellular nanoBRET assays were performed in Non-Binding Surface (NBS™)/white, 96-well plates (Corning) by addition of 1.7×10^4 cells/well (85 µL). NanoBRET Tracer 5 (Promega) was used at a final concentration of 0.25 µM as previously evaluated in a titration experiment. A total of 5 µL/well (20× working stock of nanoBRET Tracer 5 [5 µM]) was added to all wells, except the “no tracer” control wells to which 5 µL/well of tracer dilution buffer alone was added. All inhibitors were prepared initially as concentrated stock solutions in 100% DMSO (Sigma). A total of 10 µL/well of the 10× chemical inhibitor stock solutions (final assay concentration 1% DMSO) were added. For “no compound” and “no tracer” control wells, a total of 10 L/well of Opti-MEM plus DMSO (9 µL was added (final concentration 1% DMSO)). 96 well plates containing cells with nanoBRET Tracer 5 and inhibitors (100 µL total volume per well) were equilibrated (37 °C/5% CO₂) for 2 hours. To measure nanoBRET signal, nanoBRET NanoGlo substrate at a ratio of 1:166 to Opti-MEM media in combination with extracellular NanoLuc Inhibitor diluted 1:500 (10 µL [30 mM stock] per 5 mL Opti-MEM plus substrate) were combined to create a 3× stock. A total of 50 µL of the 3× substrate/extracellular NanoLuc inhibitor were added to each well. The plates were read within 15 min (GloMax Discover luminometer, Promega) equipped with 450 nm BP filter (donor) and 600 nm LP filter (acceptor), using 0.3 s integration time instrument utilizing the “nanoBRET 618” protocol.

Analysis of Inhibitors were screened at eight concentrations were evaluated in competition with NanoBRET Tracer 5 in HEK293 cells transiently expressing GAK. Prior to curve fitting, the average BRET ratio for “no tracer” (Opti-MEM + DMSO only) wells was subtracted from all experimental inhibitor well BRET ratio values and converted to mBRET units (× 1000). Additional normalization of the NanoBRET assay data was performed by converting experimental values for respective concentrations of experimental inhibitors to relative percent control values (no compound [Opti-MEM + DMSO + Tracer 5 only] wells = 100% Control, no tracer [Opti-MEM + DMSO] wells = 0% control). The data was normalized to 0% and 100% inhibition control values and fitted to a sigmoidal dose-response binding curve in GraphPad Software (version 7, La Jolla, CA, USA). Compounds that demonstrated < 10% inhibition at 5 µM were reported as no curve and compounds that showed 10% < x < 50% inhibition at 5 µM were reported as % inhibition. Compounds greater than 50% were reported as an IC₅₀ value.

Ligand binding displacement assays: Screening was performed as previously described,^[17] Briefly, inhibitor binding was determined using a binding-displacement assay, which measures the ability of inhibitors to displace a fluorescent tracer compound from the ATP

binding site of the kinase domain. Inhibitors were dissolved in DMSO and dispensed as 16-point, 2 V serial dilutions in duplicate into black multiwell plates (Greiner). Each well contained either 0.5 or 1 nM biotinylated kinase domain protein ligated to streptavidin-Tb-cryptate (Cisbio), 12.5 or 25 nM Kinase Tracer 236 (ThermoFisher Scientific), 10 mM HEPES pH 7.5, 150 mM NaCl, 2 mM DTT, 0.01% BSA, 0.01% Tween-20. Final assay volume for each data point was 5 mL, and final DMSO concentration was 1%. The kinase domain proteins were expressed in *E. coli* as a fusion with a C-terminal AVI tag (vector pNIC-Bio3, NCBI reference JN792439) which was biotinylated by co-expressed BirA, and purified using the same methods as used previously.^[17] After setting up the assay plate it was incubated at room temperature for 1.5 hours and then read using a TR-FRET proto Residue ranges were AAK1: 31–396, BMP2 K: 38–345, GAK: 12–347, STK16: 13–305 col on a PheraStarFS plate reader (BMG Labtech). The data were normalized to 0% and 100% inhibition control values and fitted to a four parameter dose-response binding curve in GraphPad Software (version 7, La Jolla, CA, USA). The determined IC₅₀ values were converted into K_i values using the Cheng-Prusoff equation and the concentration and K_d values for the tracer (previously determined). Constructs used: AAK1 – AAKA-p051; BMPK2 K – BMP2KA-p031; GAK – GAKA-p059; STK16 – STK16 A-p016.^[17]

Chemistry

X-ray crystallography: Single-crystal x-ray diffraction analyses of **13**, **14**, **25**, **27** and **29** were performed using a Rigaku FRE+ equipped with VHF Varimax confocal mirrors and an AFC12 goniometer and HyPix 6000 hybrid pixel detector equipped with an Oxford Cryosystems low temperature apparatus operating at $T=100(2)$ K. CrysAlisPro^[58] was used to record images. CrysAlisPro was used to process all data and apply empirical absorption corrections and unit cell parameters were refined against all data. The structures were solved by intrinsic phasing using SHELXT^[59] and refined on Fo2 by full-matrix least-squares refinements using SHELXL^[60] as implemented within OLEX2.^[61] All non-hydrogen atoms were refined with anisotropic displacement parameters and hydrogen atoms were added at calculated positions except those attached to heteroatoms which were located from the difference map. All hydrogen atoms were refined using a riding model with isotropic displacement parameters based on the equivalent isotropic displacement parameter (U_{eq}) of the parent atom. Figures were produced using OLEX2. The data for **14** were processed as a 2-component non-merohedral twin with the second component rotated -179.8006° around $[-0.01 \ -0.29 \ 0.96]$ (reciprocal) or $[0.00 \ 0.00 \ 1.00]$ (direct) lattice vectors. The data for **29** were processed as an inversion twin. Solvent masking was applied to the data for **13** and **25** to eliminate the electronic contribution equivalent to 1.5 and 1 molecules of water, respectively. CCDC 1982229-1982230, 1982232-1982234 contain the supplementary crystallographic data for this paper. These data are provided free of charge by The Cambridge Crystallographic Data Centre

Mass spectrometry method: Samples were analysed with a ThermoFisher Q Exactive HF-X (ThermoFisher, Bremen, Germany) mass spectrometer coupled with a Waters Acquity H-class liquid chromatograph system. Samples were introduced via a heated electrospray source (HESI) at a flow rate of 0.6 mL/min. Electrospray source conditions were set as: spray voltage 3.0 kV, sheath gas (nitrogen) 60 arb, auxiliary gas (nitrogen) 20 arb, sweep gas (nitrogen) 0 arb, nebulizer temperature 375 degrees C, capillary temperature 380 degrees C, RF funnel 45 V. The mass range was set to 150–2000 m/z. All measurements were recorded at a resolution setting of 120000.

Separations were conducted on a Waters Acquity UPLC BEH C18 column (2.1 × 50 mM, 1.7 μM particle size). LC conditions were set at 100% water with 0.1% formic acid (A) ramped linearly over 9.8 mins to 95% acetonitrile with 0.1% formic acid (B) and held until 10.2 mins. At 10.21 mins the gradient was switched back to 100% A and allowed to re-equilibrate until 11.25 mins. Injection volume for all samples was 3 μL.

Xcalibur (ThermoFisher, Bremen, Germany) was used to analyse the data. Solutions were analysed at 0.1 mg/mL or less based on responsiveness to the ESI mechanism. Molecular formula assignments were determined with Molecular Formula Calculator (v 1.2.3). All observed species were singly charged, as verified by unit m/z separation between mass spectral peaks corresponding to the ¹²C and ¹³C¹²C_{*c-1*} isotope for each elemental composition.

General procedure for the synthesis of 4-anilinoquin(az)olines: 4-chloroquin(az)oline derivative (1.0 equiv) and aniline derivative (1.1 equiv) were suspended in ethanol (10 mL) and refluxed for 18 h. The crude mixture was purified by flash chromatography using EtOAc/hexane followed by 1–5% methanol in EtOAc; After solvent removal under reduced pressure, the product was obtained as a solid or recrystallized from ethanol/water. Compounds **1–4** were prepared as previously described.^[17]

3-((6-(Trifluoromethyl)quinolin-4-yl)amino)phenol (5) was obtained as a mustard solid (114 mg, 0.376 mmol, 58%). m.p. 166–168 °C; ¹H NMR (400 MHz, [D₆]DMSO): δ = 11.09 (s, 1H), 10.05 (s, 1H), 9.32 (s, 1H), 8.56 (d, $J=6.6$ Hz, 1H), 8.39–8.11 (m, 2H), 7.32 (t, $J=8.0$ Hz, 1H), 7.13–6.61 (m, 4H). ¹³C NMR (100 MHz, [D₆]DMSO): δ = 158.8, 154.3, 145.5, 142.0, 138.3, 130.6, 128.4 (d, $J=3.5$ Hz), 126.3 (q, $J=32.7$ Hz), 125.3, 123.4, 122.5 (d, $J=5.2$ Hz), 117.0, 115.1, 114.3, 111.8, 101.4. HRMS m/z [$M+H$]⁺ calcd for C₁₆H₁₂N₂O₂F₃: 305.0902, found 305.0892, LC $t_R=3.38$ min, > 98% purity.

N-(3-Nitrophenyl)-6-(trifluoromethyl)quinolin-4-amine (6) (179 mg, 0.538 mmol, 83%) ¹H NMR (400 MHz, [D₆]DMSO): δ = 11.84 (s, 1H), 9.59–9.33 (m, 1H), 8.69 (d, $J=7.0$ Hz, 1H), 8.38 (dd, $J=4.5$, 2.4 Hz, 2H), 8.32 (dd, $J=9.0$, 1.7 Hz, 1H), 8.24 (ddd, $J=8.3$, 2.3, 1.0 Hz, 1H), 8.02 (ddd, $J=8.0$, 2.1, 1.0 Hz, 1H), 7.86 (t, $J=8.1$ Hz, 1H), 7.10 (d, $J=7.0$ Hz, 1H). ¹³C NMR (100 MHz, [D₆]DMSO): δ = 155.2, 148.6, 144.6, 140.3, 138.4, 131.4 (d, $J=17.2$ Hz), 129.4 (d, $J=3.4$ Hz), 127.8, 127.0 (q, $J=32.9$ Hz), 125.1, 123.0 (q, $J=4.1$ Hz), 122.4, 122.0 (d, $J=26.5$ Hz), 120.0, 117.1, 101.6. HRMS m/z [$M+H$]⁺ calcd for C₁₆H₁₁N₃O₂F₃: 334.0803, found 334.0793, LC $t_R=3.78$ min, > 98% purity.

N¹-(6-(Trifluoromethyl)quinolin-4-yl)benzene-1,3-diamine (7) **6** (150 mg) was treated with palladium on carbon under hydrogen for 18 h and purified by flash chromatography using EtOAc/hexane followed by 2% methanol in EtOAc. The solvent was removed under reduced pressure, the product was obtained as a dark yellow solid (94 mg, 0.311 mmol, 69%). ¹H NMR (400 MHz, [D₆]DMSO): δ = 10.79 (s, 1H), 8.86–8.72 (m, 1H), 8.47 (d, $J=6.9$ Hz, 1H), 8.09 (dd, $J=8.5$, 1.2 Hz, 1H), 7.98 (ddd, $J=8.4$, 6.9, 1.2 Hz, 1H), 7.75 (ddd, $J=8.4$, 6.9, 1.2 Hz, 1H), 7.18 (t, $J=8.0$ Hz, 1H), 6.78 (d, $J=6.9$ Hz, 1H), 6.71–6.38 (m, 3H), 5.48 (s, 2H). ¹³C NMR (100 MHz, [D₆]DMSO): δ = 154.8, 150.4, 142.6, 138.7, 137.8, 133.6, 130.2, 126.7, 123.6, 120.5, 117.0, 113.0, 112.1, 110.2, 99.9. HRMS m/z [$M+H$]⁺ calcd for C₁₆H₁₃N₃F₃: 304.1062, found 304.1051, LC $t_R=3.20$ min, > 98% purity.

¹N,¹N-Dimethyl-3-N-[6-(trifluoromethyl)quinolin-4-yl]benzene-1,3-diamine (8) was obtained as a dark yellow solid (163 mg, 0.492 mmol, 76%). m.p. decomp > 160 °C; ¹H NMR (400 MHz, [D₆]DMSO): δ = 11.37 (s, 1H), 9.36 (dt, $J=1.9$, 1.0 Hz, 1H), 8.55 (d, $J=7.1$ Hz, 1H), 8.46–8.08 (m, 2H), 7.45–7.25 (m, 1H), 6.87 (d, $J=7.1$ Hz, 1H), 6.86–6.75 (m, 2H), 6.76–6.60 (m, 1H), 2.94 (s, 6H). ¹³C NMR (101 MHz, [D₆]DMSO): δ = 155.6, 151.6, 143.8, 140.3, 137.5, 130.3, 129.2 (d, $J=3.4$ Hz), 126.6 (q, $J=32.7$ Hz), 125.1, 122.6 (q, $J=4.1$ Hz),

121.9, 116.6, 112.3, 111.6, 108.7, 101.2, 40.0 (s, 2 C). HRMS m/z [$M+H$]⁺ calcd for C₁₈H₁₇N₃F₃: 332.1375, found 332.1366, LC t_R = 4.02 min, > 98% purity.

N-(3-Nitrophenyl)quinolin-4-amine (9) was obtained as a yellow solid (217 mg, 0.816 mmol, 89%). m.p. > 250 °C; ¹H NMR (400 MHz, [D₆]DMSO): δ = 11.39 (s, 1H), 8.94 (dd, J = 8.6, 1.2 Hz, 1H), 8.61 (d, J = 6.9 Hz, 1H), 8.38 (t, J = 2.2 Hz, 1H), 8.22 (ddd, J = 8.3, 2.3, 1.0 Hz, 1H), 8.17 (dd, J = 8.6, 1.2 Hz, 1H), 8.08–8.00 (m, 2H), 7.87–7.81 (m, 2H), 7.04 (d, J = 6.8 Hz, 1H). ¹³C NMR (101 MHz, [D₆]DMSO): δ = 154.6, 148.6, 143.2, 138.9, 138.4, 134.0, 131.4, 131.2, 127.3, 124.0, 121.5, 120.4, 119.8, 117.6, 100.4. HRMS m/z [$M+H$]⁺ calcd for C₁₅H₁₂N₃O₂: 266.0930, found 266.0920, LC t_R = 2.97 min, > 98% purity.

N',N'-Dimethyl-N²-(quinolin-4-yl)benzene-1,3-diamine (10) was obtained as a dark yellow solid (188 mg, 0.715 mmol, 78%) m.p. > 250 °C; ¹H NMR (400 MHz, [D₆]DMSO): δ = 10.98 (s, 1H), 8.85 (dd, J = 8.7, 1.2 Hz, 1H), 8.47 (d, J = 7.0 Hz, 1H), 8.11 (dd, J = 8.6, 1.2 Hz, 1H), 8.00 (ddd, J = 8.4, 6.9, 1.2 Hz, 1H), 7.77 (ddd, J = 8.3, 6.9, 1.2 Hz, 1H), 7.35 (td, J = 7.8, 0.9 Hz, 1H), 6.80 (d, J = 7.0 Hz, 1H), 6.78–6.44 (m, 3H), 2.94 (s, 6H). ¹³C NMR (101 MHz, [D₆]DMSO): δ = 155.1, 151.6, 142.4, 138.3, 137.9, 133.7, 130.2, 126.8, 123.7, 120.2, 117.0, 112.5, 111.3, 109.0, 100.0, 40.0 (s, 2 C). HRMS m/z [$M+H$]⁺ calcd for C₁₇H₁₈N₃: 264.1501, found 264.1493, LC t_R = 3.09 min, > 98% purity.

(3-{{6-(Trifluoromethyl)quinolin-4-yl}amino}phenyl)methanol (11) was obtained as a light yellow solid (151 mg, 0.473 mmol, 73%). m.p. 152–154 °C; ¹H NMR (400 MHz, [D₆]DMSO): δ = 10.94 (s, 1H), 9.28 (d, J = 1.9 Hz, 1H), 8.57 (d, J = 6.6 Hz, 1H), 8.26 (d, J = 8.9 Hz, 1H), 8.19 (dd, J = 8.9, 1.8 Hz, 1H), 7.49 (t, J = 7.7 Hz, 1H), 7.43 (t, J = 1.8 Hz, 1H), 7.32 (ddt, J = 10.4, 7.6, 1.2 Hz, 2H), 6.90 (d, J = 6.6 Hz, 1H), 5.42 (s, 1H), 4.57 (s, 2H). ¹³C NMR (100 MHz, [D₆]DMSO): δ = 153.6, 146.5, 144.7, 143.0, 137.6, 129.5, 128.0 (d, J = 2.7 Hz), 126.2 (q, J = 32.7 Hz), 125.4, 124.7, 124.3, 122.4, 122.3 (d, J = 4.3 Hz), 122.3, 117.3, 101.3, 62.4. HRMS m/z [$M+H$]⁺ calcd for C₁₇H₁₄N₂OF₃: 319.1058, found 319.1048, LC t_R = 3.26 min, > 98% purity.

(2-{{6-(Trifluoromethyl)quinolin-4-yl}amino}phenyl)methanol (12) was obtained as a grey/yellow solid (132 mg, 0.416 mmol, 64%). m.p. 120–122 °C; ¹H NMR (400 MHz, [D₆]DMSO): δ = 10.18 (s, 1H), 9.18 (s, 1H), 8.48 (d, J = 6.1 Hz, 1H), 8.33–7.85 (m, 2H), 7.84–7.56 (m, 1H), 7.56–6.93 (m, 3H), 6.27 (d, J = 6.1 Hz, 1H), 5.33 (s, 1H), 4.49 (s, 2H). ¹³C NMR (100 MHz, [D₆]DMSO): δ = 152.9, 148.9, 145.7, 139.2, 135.3, 128.4, 128.2, 127.5, 127.0, 126.9–126.4 (m), 125.6 (d, J = 4.9 Hz), 125.3, 122.9, 121.8 (q, J = 4.3 Hz), 117.4, 101.3, 59.0. HRMS m/z [$M+H$]⁺ calcd for C₁₇H₁₄N₂OF₃: 319.1058, found 319.1048, LC t_R = 3.24 min, > 98% purity.

6-Bromo-N-(3-methoxyphenyl)quinolin-4-amine (13) was obtained as a beige solid (151 mg, 0.458 mmol, 74%). m.p. 188–190 °C; ¹H NMR (400 MHz, [D₆]DMSO): δ = 11.07 (s, 1H), 9.16 (d, J = 2.0 Hz, 1H), 8.52 (d, J = 7.0 Hz, 1H), 8.17 (dd, J = 9.0, 2.0 Hz, 1H), 8.08 (d, J = 9.0 Hz, 1H), 7.48 (t, J = 8.4 Hz, 1H), 7.31–7.03 (m, 2H), 7.00 (ddd, J = 8.3, 2.4, 1.0 Hz, 1H), 6.89 (d, J = 6.9 Hz, 1H), 3.81 (s, 3H). ¹³C NMR (100 MHz, [D₆]DMSO): δ = 160.3, 153.9, 143.0, 138.2, 137.4, 136.6, 130.8, 126.2, 122.5, 119.8, 118.6, 117.1, 113.1, 110.9, 100.7, 55.4. HRMS m/z [$M+H$]⁺ calcd for C₁₆H₁₄N₂BrO: 329.0286, found 329.0289, LC t_R = 3.63 min, > 98% purity.

3-((6-Bromoquinolin-4-yl)amino)phenol (14) was obtained as a yellow solid (138 mg, 0.437 mmol, 71%). m.p. > 300 °C; ¹H NMR (400 MHz, [D₆]DMSO): δ = 11.00 (s, 1H), 10.03 (s, 1H), 9.14 (d, J = 2.0 Hz, 1H), 8.51 (d, J = 7.0 Hz, 1H), 8.15 (dd, J = 9.0, 2.0 Hz, 1H), 8.06 (d, J = 9.0 Hz, 1H), 7.42–7.29 (m, 1H), 7.10–6.66 (m, 4H). ¹³C NMR (100 MHz, [D₆]DMSO): δ = 159.2, 154.4, 143.3, 138.3, 137.7, 137.0, 131.1, 126.6, 122.8, 120.2, 119.0, 115.9, 115.2, 112.5, 101.0. HRMS m/z [$M+H$]⁺ calcd for C₁₅H₁₁BrN₂O: 315.0132, found 315.0124, LC t_R = 3.01 min, > 98% purity.

m/z [$M+H$]⁺ calcd for C₁₅H₁₁BrN₂O: 315.0132, found 315.0124, LC t_R = 3.01 min, > 98% purity.

N-(3-Methoxyphenyl)quinolin-4-amine (15) was obtained as a grey solid (191 mg, 0.761 mmol, 81%). m.p. 198–200 °C; ¹H NMR (400 MHz, [D₆]DMSO): δ = 11.08 (s, 1H), 8.88 (dd, J = 8.6, 1.2 Hz, 1H), 8.50 (d, J = 7.0 Hz, 1H), 8.13 (dd, J = 8.6, 1.2 Hz, 1H), 8.02 (ddd, J = 8.4, 6.9, 1.2 Hz, 1H), 7.79 (ddd, J = 8.4, 6.9, 1.2 Hz, 1H), 7.54–7.40 (m, 1H), 7.31–7.04 (m, 2H), 7.04–6.89 (m, 1H), 6.85 (d, J = 6.9 Hz, 1H), 3.81 (s, 3H). ¹³C NMR (100 MHz, [D₆]DMSO): δ = 160.3, 154.9, 142.6, 138.4, 138.2, 133.8, 130.7, 127.0, 123.8, 120.2, 117.4, 117.1, 113.1, 111.2, 100.0, 55.4. HRMS m/z [$M+H$]⁺ calcd for C₁₆H₁₅N₂O: 251.1184, found 251.1175, LC t_R = 3.17 min, > 98% purity.

3-(Quinolin-4-ylamino)phenol (16) was obtained as a green/yellow solid (74 mg, 0.312 mmol, 34%). m.p. decomp. > 230 °C; ¹H NMR (400 MHz, [D₆]DMSO): δ = 10.97 (s, 1H), 10.03 (s, 1H), 8.84 (dd, J = 8.7, 1.1 Hz, 1H), 8.50 (d, J = 7.0 Hz, 1H), 8.11 (dd, J = 8.5, 1.2 Hz, 1H), 8.01 (ddd, J = 8.4, 6.9, 1.2 Hz, 1H), 7.77 (ddd, J = 8.3, 6.9, 1.2 Hz, 1H), 7.48–7.19 (m, 1H), 6.91–6.80 (m, 3H). ¹³C NMR (100 MHz, [D₆]DMSO): δ = 158.8, 155.0, 142.5, 138.2, 138.0, 133.8, 130.6, 126.9, 123.8, 120.1, 117.1, 115.7, 114.7, 112.3, 99.9. HRMS m/z [$M+H$]⁺ calcd for C₁₅H₁₃N₂O: 237.1028, found 237.1019, LC t_R = 2.66 min, > 98% purity.

6-Methoxy-N-(3-methoxyphenyl)quinolin-4-amine (17) was obtained as a beige/yellow solid (148 mg, 0.527 mmol, 68%). m.p. 170–172 °C; ¹H NMR (400 MHz, [D₆]DMSO): δ = 10.93 (s, 1H), 8.41 (d, J = 6.9 Hz, 1H), 8.28 (d, J = 2.6 Hz, 1H), 8.06 (d, J = 9.3 Hz, 1H), 7.66 (dd, J = 9.2, 2.6 Hz, 1H), 7.52–7.40 (m, 1H), 7.28–7.03 (m, 2H), 6.99 (ddd, J = 8.4, 2.4, 1.1 Hz, 1H), 6.84 (d, J = 6.8 Hz, 1H), 4.00 (s, 3H), 3.81 (s, 3H). ¹³C NMR (100 MHz, [D₆]DMSO): δ = 160.3, 158.0, 153.8, 140.5, 138.6, 133.5, 130.7, 125.4, 121.9, 118.5, 117.4, 112.8, 111.1, 103.0, 99.8, 56.6, 55.4. HRMS m/z [$M+H$]⁺ calcd for C₁₇H₁₇N₂O₂: 281.1290, found 281.1281, LC t_R = 3.58 min, > 98% purity.

3-((6-Methoxyquinolin-4-yl)amino)phenol (18) was obtained as a beige solid (78 mg, 0.294 mmol, 38%). m.p. > 300 °C; ¹H NMR (400 MHz, [D₆]DMSO): δ = 10.79 (s, 1H), 9.99 (s, 1H), 8.40 (d, J = 6.9 Hz, 1H), 8.23 (d, J = 2.6 Hz, 1H), 8.04 (d, J = 9.3 Hz, 1H), 7.65 (dd, J = 9.2, 2.5 Hz, 1H), 7.39–7.29 (m, 1H), 7.00–6.71 (m, 4H), 3.99 (s, 3H). ¹³C NMR (100 MHz, [D₆]DMSO): δ = 158.7, 157.9, 153.8, 140.5, 138.3, 133.5, 130.6, 125.3, 121.9, 118.4, 115.7, 114.4, 112.3, 102.9, 99.6, 56.5. HRMS m/z [$M+H$]⁺ calcd for C₁₆H₁₅N₂O₂: 267.1134, found 267.1124, LC t_R = 3.05 min, > 98% purity.

6-Methanesulfonyl-N-(3-methoxyphenyl)quinolin-4-amine (19) was obtained as a yellow solid (171 mg, 0.521 mmol, 84%). m.p. 271–273 °C; ¹H NMR (400 MHz, [D₆]DMSO): δ = 11.61 (s, 1H), 9.55 (d, J = 1.8 Hz, 1H), 8.59 (d, J = 7.0 Hz, 1H), 8.44 (dd, J = 8.9, 1.8 Hz, 1H), 8.31 (d, J = 8.9 Hz, 1H), 7.54–7.45 (m, 1H), 7.14–7.05 (m, 2H), 7.03 (ddd, J = 8.4, 2.3, 1.1 Hz, 1H), 6.95 (d, J = 7.0 Hz, 1H), 3.81 (s, 3H), 3.44 (s, 3H). ¹³C NMR (100 MHz, [D₆]DMSO): δ = 160.4, 155.6, 144.4, 140.7, 138.7, 138.0, 130.8, 130.4, 124.9, 121.8, 117.1, 116.8, 113.3, 110.9, 101.5, 55.4, 43.5. HRMS m/z [$M+H$]⁺ calcd for C₁₇H₁₇N₂O₃S: 329.0960, found 329.0953, LC t_R = 3.08 min, > 98% purity.

3-((6-(Methylsulfonyl)quinolin-4-yl)amino)phenol (20) was obtained as a yellow solid (98 mg, 0.312 mmol, 50%). m.p. > 300 °C; ¹H NMR (400 MHz, [D₆]DMSO): δ = 11.51 (s, 1H), 10.03 (s, 1H), 9.51 (d, J = 1.8 Hz, 1H), 8.58 (d, J = 7.1 Hz, 1H), 8.43 (dd, J = 8.9, 1.8 Hz, 1H), 8.28 (d, J = 8.9 Hz, 1H), 7.37 (t, J = 8.3 Hz, 1H), 7.09–6.66 (m, 4H), 3.43 (s, 3H). ¹³C NMR (100 MHz, [D₆]DMSO): δ = 158.8, 155.6, 144.2, 140.7, 138.6, 137.8, 130.7, 130.4, 124.9, 121.8, 116.8, 115.4, 114.9, 112.0, 101.3, 43.5. HRMS m/z [$M+H$]⁺ calcd for C₁₆H₁₅N₂O₃S: 315.0803, found 315.0796, LC t_R = 2.29 min, > 98% purity.

6-Bromo-N-(3-nitrophenyl)quinolin-4-amine (21) was obtained as a beige solid (162 mg, 0.470 mmol, 76%). m.p. 290–292 °C; ¹H NMR

(400 MHz, [D₆]DMSO): δ = 11.39 (s, 1H), 9.23 (d, J = 2.0 Hz, 1H), 8.62 (d, J = 6.9 Hz, 1H), 8.36 (t, J = 2.2 Hz, 1H), 8.30–8.15 (m, 2H), 8.13 (d, J = 9.0 Hz, 1H), 8.00 (ddd, J = 8.0, 2.1, 1.0 Hz, 1H), 7.84 (t, J = 8.1 Hz, 1H), 7.08 (d, J = 6.9 Hz, 1H). ¹³C NMR (100 MHz, [D₆]DMSO): δ = 153.6, 148.6, 143.5, 138.6, 137.5, 136.7, 131.3, 131.2, 126.4, 122.6, 121.6, 120.2, 119.7, 119.0, 101.1. HRMS m/z [M+H]⁺ calcd for C₁₅H₁₁N₃O₂Br: 344.0035, found 344.0032, LC t_R = 3.48 min, > 98% purity.

1-*N*-(6-Bromoquinolin-4-yl)benzene-1,3-diamine (22) (150 mg) was treated with palladium on carbon under hydrogen for 18 h and purified by flash chromatography using EtOAc/hexane followed by 2% methanol in EtOAc. The solvent was removed under reduced pressure, the product was obtained as a brown solid (129 mg, 0.410 mmol, 94%). m.p. 280–282 °C; ¹H NMR (400 MHz, [D₆]DMSO): δ = 11.06 (s, 1H), 8.85 (d, J = 8.6 Hz, 1H), 8.58 (d, J = 6.9 Hz, 1H), 8.16–8.00 (m, 2H), 7.81 (t, J = 7.8 Hz, 1H), 7.57 (t, J = 8.2 Hz, 1H), 7.34 (d, J = 6.0 Hz, 2H), 7.24 (d, J = 7.7 Hz, 1H), 6.89 (d, J = 6.9 Hz, 1H). ¹³C NMR (100 MHz, [D₆]DMSO): δ = 154.8, 142.8, 138.2, 138.1, 134.0, 130.9, 127.2, 123.8, 123.6, 121.6, 120.2, 119.8, 117.6, 117.2, 100.0. HRMS m/z [M+H]⁺ calcd for C₁₅H₁₃BrN₃: 314.0293, found 314.0293, LC t_R = 2.22 min, > 98% purity.

3-*N*-(6-Bromoquinolin-4-yl)-1-*N*,1-*N*-dimethylbenzene-1,3-diamine (23) was obtained as a yellow/mustard solid (144 mg, 0.421 mmol, 68%). m.p. Decomp. > 280 °C; ¹H NMR (400 MHz, [D₆]DMSO): δ = 10.99 (s, 1H), 9.14 (d, J = 2.0 Hz, 1H), 8.48 (d, J = 6.9 Hz, 1H), 8.15 (dd, J = 9.0, 2.0 Hz, 1H), 8.07 (d, J = 9.0 Hz, 1H), 7.39–7.27 (m, 1H), 6.84 (d, J = 7.0 Hz, 1H), 6.81–6.51 (m, 3H), 2.94 (s, 6H). ¹³C NMR (100 MHz, [D₆]DMSO): δ = 154.2, 151.6, 142.8, 137.7, 137.3, 136.5, 130.2, 126.1, 122.4, 119.7, 118.5, 112.2, 111.38, 108.7, 100.6, 39.98 (2 C, s). HRMS m/z [M+H]⁺ calcd for C₁₇H₁₇N₃Br: 342.0606, found 342.0597, LC t_R = 3.74 min, > 98% purity.

3-[(6-Bromoquinolin-4-yl)amino]phenyl)methanol (24) was obtained as a yellow/mustard solid (155 mg, 0.470 mmol, 76%). m.p. 132–134 °C; ¹H NMR (400 MHz, [D₆]DMSO): δ = 10.93 (s, 1H), 9.13 (d, J = 2.0 Hz, 1H), 8.52 (d, J = 6.8 Hz, 1H), 8.14 (dd, J = 9.0, 1.9 Hz, 1H), 8.06 (d, J = 9.0 Hz, 1H), 7.51 (t, J = 7.7 Hz, 1H), 7.45–7.11 (m, 3H), 6.85 (d, J = 6.8 Hz, 1H), 5.41 (s, 1H), 4.58 (s, 2H). ¹³C NMR (100 MHz, [D₆]DMSO): δ = 153.5, 144.8, 143.6, 138.1, 137.1, 136.2, 129.6, 126.1, 125.1, 123.1, 122.7, 119.7, 118.8, 100.5, 62.3. HRMS m/z [M+H]⁺ calcd for C₁₆H₁₄N₂OBr: 329.0289, found 329.0283, LC t_R = 4.20 min, > 98% purity.

***N*-(2*H*-1,3-Benzodioxol-5-yl)-6-bromoquinolin-4-amine (25)** was obtained as a green solid (144 mg, 0.421 mmol, 68%). m.p. 240–242 °C; ¹H NMR (400 MHz, [D₆]DMSO): δ = 11.00 (s, 1H), 9.14 (d, J = 2.0 Hz, 1H), 8.49 (d, J = 7.0 Hz, 1H), 8.15 (dd, J = 9.0, 2.0 Hz, 1H), 8.06 (d, J = 9.0 Hz, 1H), 7.44–7.00 (m, 2H), 6.93 (dd, J = 8.2, 2.1 Hz, 1H), 6.73 (d, J = 6.9 Hz, 1H), 6.13 (s, 2H). ¹³C NMR (100 MHz, [D₆]DMSO): δ = 154.5, 148.2, 146.6, 142.8, 137.3, 136.5, 130.6, 126.2, 122.4, 119.7, 119.2, 118.4, 108.9, 106.9, 101.9, 100.4. HRMS m/z [M+H]⁺ calcd for C₁₆H₁₂N₂O₂Br: 343.0082, found 343.0079, LC t_R = 3.49 min, > 98% purity.

6-Bromo-*N*-(1,3-dihydro-2-benzofuran-5-yl)quinolin-4-amine (26) was obtained as a yellow solid (148 mg, 0.433 mmol, 70%). m.p. 140–142 °C; ¹H NMR (400 MHz, [D₆]DMSO): δ = 11.22 (s, 1H), 9.22 (d, J = 2.0 Hz, 1H), 8.49 (d, J = 7.0 Hz, 1H), 8.14 (dd, J = 9.0, 1.9 Hz, 1H), 8.08 (d, J = 9.0 Hz, 1H), 7.48 (d, J = 7.8 Hz, 1H), 7.42 (d, J = 2.0 Hz, 1H), 7.37 (dd, J = 8.0, 1.9 Hz, 1H), 6.80 (d, J = 7.0 Hz, 1H), 5.05 (s, 4H). ¹³C NMR (100 MHz, [D₆]DMSO): δ = 154.6, 143.3, 141.5, 138.8, 137.7, 137.0, 136.6, 126.7, 125.0, 123.0, 122.8, 120.3, 119.0, 118.8, 100.8, 72.93, 72.86. HRMS m/z [M+H]⁺ calcd for C₁₇H₁₄N₂OBr: 341.0289, found 341.0286, LC t_R = 3.28 min, > 98% purity.

***N*-(Benzo[d][1,3]dioxol-4-yl)-6-bromoquinolin-4-amine (27)** was obtained as a yellow solid (157 mg, 0.458 mmol, 74%). m.p.

> 270 °C decomp.; ¹H NMR (400 MHz, [D₆]DMSO): δ = 11.21 (s, 1H), 9.24 (d, J = 1.9 Hz, 1H), 8.57 (d, J = 6.9 Hz, 1H), 8.25–8.02 (m, 2H), 7.16–6.81 (m, 3H), 6.65 (d, J = 6.9 Hz, 1H), 6.11 (s, 2H). ¹³C NMR (101 MHz, [D₆]DMSO): δ = 153.1, 148.8, 142.9, 141.5, 137.2, 136.5, 126.3, 122.6, 122.5, 120.0, 119.5, 119.1, 118.4, 107.9, 101.84, 101.80. HRMS m/z [M+H]⁺ calcd for C₁₆H₁₂N₂O₂Br: 343.0082, found 343.0072, LC t_R = 3.43 min, > 98% purity.

6-Bromo-*N*-(1,3-dihydro-2-benzofuran-4-yl)quinolin-4-amine (28) was obtained as a yellow/mustard solid (141 mg, 0.414 mmol, 67%). m.p. Decomp. > 220 °C; ¹H NMR (400 MHz, [D₆]DMSO): δ = 10.81 (s, 1H), 9.16 (d, J = 1.9 Hz, 1H), 8.49 (d, J = 6.6 Hz, 1H), 8.13–7.97 (m, 2H), 7.47 (t, J = 7.6 Hz, 1H), 7.35 (ddd, J = 21.1, 7.6, 0.9 Hz, 2H), 6.47 (d, J = 6.5 Hz, 1H), 5.10 (d, J = 2.0 Hz, 2H), 4.95 (d, J = 2.0 Hz, 2H). ¹³C NMR (100 MHz, [D₆]DMSO): δ = 152.3, 144.9, 141.8, 139.6, 135.6, 135.4, 131.6, 129.3, 126.2, 124.7, 124.4, 120.2, 119.4, 119.1, 101.0, 73.0, 71.5. HRMS m/z [M+H]⁺ calcd for C₁₇H₁₄N₂OBr: 341.0289, found 341.0281, LC t_R = 3.25 min, > 98% purity.

6-Bromo-*N*-(3-methoxyphenyl)quinazolin-4-amine (29) was obtained as a light yellow solid (175 mg, 0.530 mmol, 86%). m.p. 239–241 °C; ¹H NMR (400 MHz, [D₆]DMSO): δ = 11.79 (s, 1H), 9.34 (d, J = 2.0 Hz, 1H), 8.95 (s, 1H), 8.24 (dd, J = 8.9, 2.0 Hz, 1H), 7.98 (d, J = 8.9 Hz, 1H), 7.55–7.18 (m, 3H), 6.97–6.83 (m, 1H), 3.79 (s, 3H). ¹³C NMR (100 MHz, [D₆]DMSO): δ = 159.4, 158.8, 151.1, 138.8, 138.1, 137.6, 129.5, 127.4, 122.0, 121.0, 116.7, 115.1, 112.0, 110.6, 55.3. HRMS m/z [M+H]⁺ calcd for C₁₅H₁₃N₃OBr: 330.0242, found 330.0246, LC t_R = 4.80 min, > 98% purity.

3-[(6-Bromoquinazolin-4-yl)amino]phenol (30) was obtained as a yellow solid (154 mg, 0.487 mmol, 79%). m.p. Decomp. > 250 °C; ¹H NMR (400 MHz, [D₆]DMSO): δ = 11.63 (s, 1H), 9.82 (s, 1H), 9.27 (d, J = 2.0 Hz, 1H), 8.94 (s, 1H), 8.23 (dd, J = 8.9, 2.0 Hz, 1H), 7.96 (d, J = 8.9 Hz, 1H), 7.43–6.92 (m, 3H), 6.76 (ddd, J = 8.1, 2.4, 1.0 Hz, 1H). ¹³C NMR (100 MHz, [D₆]DMSO): δ = 158.7, 157.7, 151.1, 138.7, 138.1, 137.4, 129.4, 127.3, 122.1, 120.9, 115.2, 115.1, 113.9, 111.7. HRMS m/z [M+H]⁺ calcd for C₁₄H₁₁N₃OBr: 316.0085, found 316.0081, LC t_R = 4.20 min, > 98% purity.

6-Bromo-*N*-[3-(2*H*-1,2,3,4-tetrazol-5-yl)phenyl]quinazolin-4-amine (31) was obtained as a light beige solid (184 mg, 0.499 mmol, 81%). ¹H NMR (400 MHz, [D₆]DMSO): δ = 11.21 (s, 1H), 9.18 (d, J = 2.0 Hz, 1H), 8.58 (d, J = 6.9 Hz, 1H), 8.23 (t, J = 1.9 Hz, 1H), 8.19 (dd, J = 9.0, 2.0 Hz, 1H), 8.13 (dt, J = 7.8, 1.3 Hz, 1H), 8.08 (d, J = 9.0 Hz, 1H), 7.80 (t, J = 7.9 Hz, 1H), 7.72 (ddd, J = 8.1, 2.2, 1.1 Hz, 1H), 7.02 (d, J = 6.9 Hz, 1H). ¹³C NMR (100 MHz, [D₆]DMSO): δ = 153.8, 143.4, 138.1, 137.4, 136.7, 131.1, 127.6, 126.2, 126.0, 125.7, 123.4, 122.6, 120.1, 118.8, 100.8. m.p. Decomp. 300 °C; HRMS m/z [M+H]⁺ calcd for C₁₅H₁₆N₆Br: 359.0620, found 369.0276, LC t_R = 3.10 min, > 98% purity.

6-Bromo-*N*-(3-(pentafluoro- λ^6 -sulfanyl)phenyl)quinolin-4-amine (32) was obtained as a colourless solid (200 mg, 0.470 mmol, 76%). m.p. 290–292 °C; ¹H NMR (400 MHz, [D₆]DMSO): δ = 11.31 (s, 1H), 9.18 (d, J = 2.0 Hz, 1H), 8.61 (d, J = 6.9 Hz, 1H), 8.20 (dd, J = 9.0, 2.0 Hz, 1H), 8.12 (d, J = 9.0 Hz, 1H), 8.07 (t, J = 2.0 Hz, 1H), 7.95 (ddd, J = 8.0, 2.3, 1.2 Hz, 1H), 7.86 (dt, J = 8.1, 1.5 Hz, 1H), 7.81 (t, J = 8.0 Hz, 1H), 6.96 (d, J = 6.9 Hz, 1H). ¹³C NMR (100 MHz, [D₆]DMSO): δ = 153.8, 153.5 (t, J = 16.7 Hz), 143.5, 138.2, 137.4, 136.7, 131.0, 129.0, 126.3, 124.3, 122.6, 122.6, 120.1, 118.9, 100.9. HRMS m/z [M+H]⁺ calcd for C₁₅H₁₁N₂SF₅Br: 424.9746, found 424.9736, LC t_R = 4.64 min, > 98% purity.

6-Bromo-*N*-[3-(*tert*-butoxy)phenyl]quinolin-4-amine (33) was obtained as a colourless solid (170 mg, 0.458 mmol, 74%). m.p. 280–282 °C; ¹H NMR (400 MHz, [D₆]DMSO): δ = 11.10 (s, 1H), 9.17 (d, J = 2.0 Hz, 1H), 8.54 (d, J = 6.9 Hz, 1H), 8.17 (dd, J = 9.0, 2.0 Hz, 1H), 8.08 (d, J = 9.0 Hz, 1H), 7.47 (t, J = 8.0 Hz, 1H), 7.19 (ddd, J = 7.9, 2.1, 0.9 Hz, 1H), 7.09 (t, J = 2.2 Hz, 1H), 7.03 (ddd, J = 8.2, 2.4, 0.9 Hz, 1H),

6.84 (d, $J=6.9$ Hz, 1H), 1.35 (s, 9H). ^{13}C NMR (101 MHz, $[\text{D}_6]\text{DMSO}$): $\delta=156.3, 154.0, 143.0, 137.6, 137.3, 136.6, 130.2, 126.2, 122.5, 122.4, 120.1, 119.8, 119.7, 118.6, 100.5, 78.8, 28.5$ (s, 3 C). HRMS m/z $[M+H]^+$ calcd for $\text{C}_{19}\text{H}_{20}\text{N}_2\text{OBr}$: 371.0759, found 371.0750, LC $t_R=4.54$ min, >98% purity.

6-Bromo-*N*-(3-*tert*-butylphenyl)quinolin-4-amine (34) was obtained as a yellow solid (171 mg, 0.483 mmol, 78%). m.p. 285–287 °C; ^1H NMR (400 MHz, $[\text{D}_6]\text{DMSO}$): $\delta=11.08$ (s, 1H), 9.17 (d, $J=2.0$ Hz, 1H), 8.51 (d, $J=7.0$ Hz, 1H), 8.17 (dd, $J=9.0, 2.0$ Hz, 1H), 8.08 (d, $J=9.0$ Hz, 1H), 7.86–7.37 (m, 3H), 7.31 (ddd, $J=7.4, 2.2, 1.3$ Hz, 1H), 6.83 (d, $J=7.0$ Hz, 1H), 1.32 (s, 9H). ^{13}C NMR (100 MHz, $[\text{D}_6]\text{DMSO}$): $\delta=154.0, 152.9, 143.0, 137.3, 136.7, 136.5, 129.6, 126.2, 124.4, 122.4, 122.2, 119.77, 118.6, 100.3, 34.7, 31.0$. HRMS m/z $[M+H]^+$ calcd for $\text{C}_{19}\text{H}_{20}\text{N}_2\text{Br}$: 355.0810, found 355.0800, LC $t_R=4.99$ min, >98% purity.

Acknowledgements

The SGC is a registered charity (no. 1097737) that receives funds from AbbVie, Bayer Pharma AG, Boehringer Ingelheim, Canada Foundation for Innovation, Eshelman Institute for Innovation, Genome Canada, Innovative Medicines Initiative (EU/EFPIA) [ULTRA-DD grant no. 115766], Janssen, Merck KGaA Darmstadt Germany, MSD, Novartis Pharma AG, Ontario Ministry of Economic Development and Innovation, Pfizer, São Paulo Research Foundation-FAPESP, Takeda, and Wellcome [106169/ZZ14/Z]. We also thank CSC – IT Center for Science Ltd. Finland for the use of their facilities, software licenses, computational resources and the Biocenter Finland/DDCB for financial support. The authors thank Prof. Lee Graves (University of North Carolina at Chapel Hill) for useful discussions. We are grateful to Dr. Brandie Ehrmann for LC-MS/HRMS support provided by the Mass Spectrometry Core Laboratory at the University of North Carolina at Chapel Hill. We also thank the EPSRC UK National Crystallography Service for funding and collection of the crystallographic data for 13, 14, 25, 27 and 29.

Conflict of Interest

The authors declare no conflict of interest.

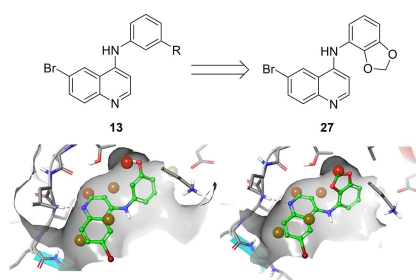
Keywords: anilinoquinazolines · anilinoquinolines · cyclin G-associated kinase (GAK) · water networks · WaterMap

- [1] E. D. Scheeff, P. E. Bourne, *PLoS Comput. Biol.* **2005**, *5*, e49.
- [2] Z. A. Knight, K. M. Shokat, *Chem. Biol.* **2005**, *12*, 621–637.
- [3] G. Manning, D. B. Whyte, R. Martinez, T. Hunter, S. Sudarsanam, *Science* **2002**, *298*, 1912–1934.
- [4] P. Badrinarayan, G. N. Sastry, *Curr. Pharm. Des.* **2013**, *19*, 4714–4738.
- [5] S. Lu, X. He, D. Ni, J. Zhang, *J. Med. Chem.* **2019**, *62*, 6405–6421.
- [6] Q. Liu, Y. Sabnis, Z. Zhao, T. Zhang, S. J. Buhrlage, L. H. Jones, N. S. Gray, *Chem. Biol.* **2013**, *20*, 146–159.
- [7] W. D. Jang, J. Kim, N. S. Kang, *J. Mol. Liq.* **2014**, *191*, 37–41.
- [8] W. D. Jang, M. H. Lee, N. S. Kang, *J. Mol. Liq.* **2016**, *221*, 361–322.
- [9] F. Heider, T. Pansar, M. Kudolo, F. Ansideri, A. De Simone, L. Pruccoli, T. Schneider, M. I. Goettert, A. Tarozzi, V. Andrisano, S. A. Laufer, P. Koch, *ACS Med. Chem. Lett.* **2019**, *10*, 1407–1414.

- [10] S. Riniker, L. J. Barandun, F. Diederich, O. Krämer, A. Steffen, W. F. van Gunsteren, *J. Comput.-Aided Mol. Des.* **2012**, *26*, 1293–1309.
- [11] R. Abel, L. Wang, R. A. Friesner, B. J. Berne, *J. Chem. Theory Comput.* **2010**, *6*, 2924–2934.
- [12] Y. Yang, F. C. Lightstone, S. E. Wong, *Expert Opin. Drug Discovery* **2013**, *8*, 277–287.
- [13] D. D. Robinson, W. Sherman, R. Farid, *ChemMedChem.* **2010**, *5*, 618–627.
- [14] S. Kannan, M. R. Pradhan, G. Tiwari, W. C. Tan, B. Chowbay, E. H. Tan, D. S. Tan, C. Verma, *Sci. Rep.* **2017**, *7*, 1540.
- [15] R. Horbert, B. Pinchuk, E. Johannes, J. Schlosser, D. Schmidt, D. Cappel, F. Totzke, C. Schächtele, C. Peifer, *J. Med. Chem.* **2015**, *58*, 170–182.
- [16] N. M. Levinson, S. G. Boxer, *Nat. Chem. Biol.* **2014**, *10*, 127–132.
- [17] C. R. M. Asquith, T. Laitinen, J. M. Bennett, P. H. Godoi, M. P. East, G. J. Tizzard, L. M. Graves, G. L. Johnson, R. E. Dornsife, C. I. Wells, J. M. Elkins, T. M. Willson, W. J. Zuercher, *ChemMedChem* **2018**, *13*, 48–66.
- [18] C. R. M. Asquith, B. T. Berger, J. Wan, J. M. Bennett, S. J. Capuzzi, D. J. Crona, D. H. Drewry, M. P. East, J. M. Elkins, O. Fedorov, P. H. Godoi, D. M. Hunter, S. Knapp, S. Müller, C. D. Torrice, C. I. Wells, H. S. Earp, T. M. Willson, W. J. Zuercher, *J. Med. Chem.* **2019**, *62*, 2830–2836.
- [19] C. R. M. Asquith, D. K. Treiber, W. J. Zuercher, *Bioorg. Med. Chem. Lett.* **2019**, *29*, 1727–1731.
- [20] C. R. M. Asquith, T. Laitinen, J. M. Bennett, C. I. Wells, J. M. Elkins, W. J. Zuercher, G. J. Tizzard, A. Poso, *ChemMedChem.* **2020**, *15*, 26–49.
- [21] F. J. Sorrell, M. Szklarz, K. R. Abdul Azeez, J. M. Elkins, S. Knapp, *Structure* **2016**, *24*, 401–411.
- [22] H. Shimizu, I. Nagamori, N. Yabuta, H. Nojima, *J. Cell Sci.* **2009**, *122*, 3145–3152.
- [23] N. Dzamko, J. Zhou, Y. Huang, G. M. Halliday, *Front. Mol. Neurosci.* **2014**, *7*, 57.
- [24] M. Sosa, E. Choy, X. Liu, J. Schwab, F. J. Hornicek, H. Mankin, Z. Duan, *Mol. Cancer Ther.* **2010**, *9*, 3342–3350.
- [25] M. R. Ray, L. A. Wafa, H. Cheng, R. Snoek, L. Fazli, M. Gleave, P. S. Rennie, *Int. J. Cancer* **2006**, *118*, 1108–1119.
- [26] S. Knapp, P. Arruda, J. Blagg, S. Burley, D. H. Drewry, A. Edwards, D. Fabbro, P. Gillespie, N. S. Gray, B. Kuster, K. E. Lackey, P. Mazzafera, N. C. Tomkinson, T. M. Willson, P. Workman, W. J. Zuercher, *Nat. Chem. Biol.* **2013**, *9*, 3–6.
- [27] S. Kovackova, L. Chang, E. Bekerman, G. Neveu, R. Barouch-Bentov, A. Chaikuad, C. Heroven, M. Sala, S. De Jonghe, S. Knapp, S. Einav, P. Herdewijn, *J. Med. Chem.* **2015**, *58*, 3393–3410.
- [28] S. Y. Pu, R. Wouters, S. Schor, J. Rozenski, R. Barouch-Bentov, L. I. Prugar, C. M. O'Brien, J. M. Brannan, J. M. Dye, P. Herdewijn, S. De Jonghe, S. Einav, *J. Med. Chem.* **2018**, *61*, 6178–6192.
- [29] C. H. Arrowsmith, J. E. Audia, C. Austin, J. Baell, J. Bennett, J. Blagg, C. Bountra, P. E. Brennan, P. J. Brown, M. E. Bunnage, C. Buser-Doepner, R. M. Campbell, A. J. Carter, P. Cohen, R. A. Copeland, B. Cravatt, J. L. Dahlin, D. Dhanak, A. M. Edwards, M. Frederiksen, S. V. Frye, N. Gray, C. E. Grimshaw, D. Hepworth, T. Howe, K. V. Huber, J. Jin, S. Knapp, J. D. Kotz, R. G. Kruger, D. Lowe, M. M. Mader, B. Marsden, A. Mueller-Fahnow, S. Müller, R. C. O'Hagen, J. P. Overington, D. R. Owen, S. H. Rosenberg, B. Roth, R. Ross, M. Schapira, S. L. Schreiber, B. Shoicet, M. Sundström, G. Superti-Furga, J. Taunton, L. Toledo-Sherman, C. Walpole, M. A. Walters, T. M. Wilson, P. Workman, R. N. Young, W. J. Zuercher, *Nat. Chem. Biol.* **2015**, *11*, 536–542.
- [30] M. A. Fabian, W. H. Biggs III, D. K. Treiber, C. E. Atteridge, M. D. Azimioara, M. G. Benedetti, T. A. Carter, P. Ciceri, P. T. Edeen, M. Floyd, J. M. Ford, M. Galvin, J. L. Gerlach, R. M. Grotzfeld, S. Herrgard, D. E. Insko, M. A. Insko, A. G. Lai, J. M. Lelias, S. A. Mehta, Z. V. Milanov, A. M. Velasco, L. M. Wodicka, H. K. Patel, P. P. Zarrinkar, D. J. Lockhart, *Nat. Biotechnol.* **2005**, *23*, 329–336.
- [31] R. Jr Roskoski, *Pharmacol. Res.* **2016**, *103*, 26–48.
- [32] R. Newton, K. A. Bowler, E. M. Burns, P. J. Chapman, E. E. Fairweather, S. J. R. Fritzl, K. M. Goldberg, N. M. Hamilton, S. V. Holt, G. V. Hopkins, S. D. Jones, A. M. Jordan, A. J. Lyons, H. Nikki March, N. Q. McDonald, L. A. Maguire, D. P. Mould, A. G. Purkiss, H. F. Small, A. I. J. Stowell, G. J. Thomson, I. D. Waddell, B. Waszkowycz, A. J. Watson, D. J. Ogilvie, *Eur. J. Med. Chem.* **2016**, *13*, 20–32.
- [33] C. R. M. Asquith, N. Fleck, C. D. Torrice, D. J. Crona, C. Grundner, W. J. Zuercher, *Bioorg. Med. Chem. Lett.* **2019**, *18*, 2695–2699.
- [34] C. R. M. Asquith, K. M. Naegeli, M. P. East, T. Laitinen, T. M. Havener, C. I. Wells, G. L. Johnson, D. H. Drewry, W. J. Zuercher, D. C. Morris, *J. Med. Chem.* **2019**, *62*, 4772–4778.
- [35] T. Machleidt, C. C. Woodrooffe, M. K. Schwinn, J. Méndez, M. B. Robers, K. Zimmerman, P. Otto, D. L. Daniels, T. A. Kirkland, K. V. Wood, *ACS Chem. Biol.* **2015**, *10*, 1797–1804.

- [36] J. D. Vasta, C. R. Corona, J. Wilkinson, C. A. Zimprich, J. R. Hartnett, M. R. Ingold, K. Zimmerman, T. Machleidt, T. A. Kirkland, K. G. Huwiler, R. F. Ohana, M. Slater, P. Otto, M. Cong, C. I. Wells, B. T. Berger, T. Hanke, C. Glas, K. Ding, D. H. Drewry, K. V. M. Huber, T. M. Willson, S. Knapp, S. Müller, P. L. Meisenheimer, F. Fan, K. V. Wood, M. B. Robers, *Cell Chem. Biol.* **2018**, *25*, 206–214.
- [37] W. F. Baitinger, P. von R. Schleyer, T. S. S. R. Murty, L. Robinson, *Tetrahedron* **1964**, *20*, 1635–1647.
- [38] L. Pauling, *J. Am. Chem. Soc.* **1932**, *54*, 3570–3582.
- [39] P. R. Savoie, J. T. Welch, *Chem. Rev.* **2015**, *115*, 1130–1190.
- [40] Schrödinger Maestro software package, Small-Molecule Drug Discovery Suite 2018-4, Schrödinger, LLC, New York, NY **2018**.
- [41] P. Politzer, J. S. Murray, T. Clark, *Phys. Chem. Chem. Phys.* **2013**, *15*, 11178–11189.
- [42] L. Wang, B. J. Berne, R. A. Friesner, *Proc. Natl. Acad. Sci. USA* **2011**, *108*, 1326–1330.
- [43] a) F. M. Ferguson, N. S. Gray, *Nat. Rev. Drug Discovery* **2018**, *17*, 353–377; b) <http://www.brimr.org/PKI/PKIs.htm>.
- [44] P. Cohen, D. R. Alessi, *ACS Chem. Biol.* **2013**, *8*, 96–104.
- [45] A. F. Rudolf, T. Skovgaard, S. Knapp, L. J. Jensen, J. Berthelsen, *PLoS One* **2014**, *9*, e98800.
- [46] M. I. Davis, J. P. Hunt, S. Herrgard, P. Ciceri, L. M. Wodicka, G. Pallares, M. Hocker, D. K. Treiber, P. P. Zarrinkar, *Nat. Biotechnol.* **2011**, *29*, 1046–1051.
- [47] H. Ma, S. Deacon, K. Horiuchi, *Expert Opin. Drug Discovery* **2008**, *3*, 607–621.
- [48] a) A. J. Kooistra, G. K. Kanev, O. P. van Linden, R. Leurs, I. J. de Esch, C. de Graaf, *Nucleic Acids Res.* **2016**, *44*, D365–D371; b) O. P. van Linden, A. J. Kooistra, R. Leurs, I. J. de Esch, C. de Graaf, *J. Med. Chem.* **2014**, *57*, 249–277.
- [49] D. Robinson, T. Bertrand, J. C. Carry, F. Halley, A. Karlsson, M. Mathieu, H. Minoux, M. A. Perrin, B. Robert, L. Schio, W. Sherman, *J. Chem. Inf. Model.* **2016**, *56*, 886–894.
- [50] P. Czodrowski, G. Hölzemann, G. Barnickel, H. Greiner, D. Musil, *J. Med. Chem.* **2015**, *58*, 457–465.
- [51] V. Myrianthopoulos, M. Kritsanida, N. Gaboriaud-Kolar, P. Magiatis, Y. Ferandin, E. Durieu, O. Lozach, D. Cappel, M. Soundararajan, P. Filippakopoulos, W. Sherman, S. Knapp, L. Meijer, E. Mikros, A. L. Skaltsounis, *ACS Med. Chem. Lett.* **2013**, *4*, 22–26.
- [52] N. Ohbayashi, K. Murayama, M. Kato-Murayama, M. Kukimoto-Niino, T. Uejima, T. Matsuda, N. Ohsawa, S. Yokoyama, H. Nojima, M. Shirouzu, *ChemistryOpen* **2018**, *7*, 721–727.
- [53] T. Young, R. Abel, B. Kim, B. J. Berne, R. A. Friesner, *Proc. Natl. Acad. Sci. USA* **2007**, *104*, 808–813.
- [54] R. Abel, T. Young, R. Farid, B. J. Berne, R. A. Friesner, *J. Am. Chem. Soc.* **2008**, *130*, 2817–2831.
- [55] D. Cappel, W. Sherman, T. Beuming, *Curr. Top. Med. Chem.* **2017**, *17*, 2586–2598.
- [56] E. Harder, W. Damm, J. Maple, C. Wu, M. Reboul, J. Y. Xiang, L. Wang, D. Lupyan, M. K. Dahlgren, J. L. Knight, J. W. Kaus, D. S. Cerutti, G. Krilov, W. L. Jorgensen, R. Abel, R. A. Friesner, *J. Chem. Theory Comput.* **2016**, *12*, 281–296.
- [57] C. R. M. Asquith, J. M. Bennett, L. Su, T. Laitinen, J. M. Elkins, J. E. Pickett, C. I. Wells, Z. Li, T. M. Willson, W. J. Zuercher, *Molecules* **2019**, *24*, 4016.
- [58] *CrysAlisPro Software System*, Rigaku Oxford Diffraction **2018**.
- [59] G. M. Sheldrick, *Acta Crystallogr. Sect. A* **2015**, *71*, 3–8.
- [60] G. M. Sheldrick, *Acta Crystallogr. Sect. C* **2015**, *71*, 3–8.
- [61] O. V. Dolomanov, L. J. Bourhis, R. J. Gildea, J. A. K. Howard, H. Puschmann, *J. Appl. Crystallogr.* **2009**, *42*, 339–341.
-

Navigating water ways: To understand better how water networks influence drugs in general and kinase inhibitors in particular, we have elucidated the properties of a proposed water network with cyclin G-associated kinase (GAK) by using a targeted point mutation library. This can be used as a tool towards more potent GAK inhibitors and to enhance wider inhibitor design.



Dr. C. R. M. Asquith*, Dr. G. J. Tizzard,
J. M. Bennett, C. I. Wells, Dr. J. M.
Elkins, Prof. T. M. Willson, Prof. A. Poso,
Dr. T. Laitinen

1 – 17

**Targeting the Water Network in
Cyclin G-Associated Kinase (GAK)
with 4-Anilino-quin(az)oline Inhibi-
tors**



Targeting the water network in cyclin G-associated kinase (GAK) with 4-anilino-quin(az)oline inhibitors (Asquith et al. @UNCRResearch @TropMedOxford @UniEastFinland @uni_tue OK?)

Share your work on social media! *ChemMedChem* has added Twitter as a means to promote your article. Twitter is an online microblogging service that enables its users to send and read short messages and media, known as tweets. Please check the pre-written tweet in the galley proofs for accuracy. If you, your team, or institution have a Twitter account, please include its handle @username. Please use hashtags only for the most important keywords, such as #catalysis, #nanoparticles, or #proteindesign. The ToC picture and a link to your article will be added automatically, so the **tweet text must not exceed 250 characters**. This tweet will be posted on the journal's Twitter account (follow us @ChemMedChem) upon publication of your article in its final (possibly unpaginated) form. We recommend you to re-tweet it to alert more researchers about your publication, or to point it out to your institution's social media team.

ORCID (Open Researcher and Contributor ID)

Please check that the ORCID identifiers listed below are correct. We encourage all authors to provide an ORCID identifier for each coauthor. ORCID is a registry that provides researchers with a unique digital identifier. Some funding agencies recommend or even require the inclusion of ORCID IDs in all published articles, and authors should consult their funding agency guidelines for details. Registration is easy and free; for further information, see <http://orcid.org/>.

Carrow I. Wells
James M. Bennett
Dr. Graham J. Tizzard
Dr. Tuomo Laitinen
Prof. Antti Poso
Dr. Jonathan M. Elkins
Prof. Timothy M. Willson
Dr. Christopher R. M. Asquith <http://orcid.org/0000-0001-5871-3458>